DEVELOPMENTAL DYNAMICS 239:2962–2979, 2010

RESEARCH ARTICLE

Cellular Response After Crush Injury in Adult Zebrafish Spinal Cord

Subhra Prakash Hui,[1] Anindita Dutta,[2] and Sukla Ghosh[1]*

Zebrafish proves to be an excellent model system to study spinal cord regeneration because it can repair its disengaged axons and replace lost cells after injury, allowing the animal to make functional recovery. We have characterized injury response following crush injury, which is comparable to the mammalian mode of injury. Infiltrations of blood cells during early phases involve macrophages that are important in debris clearance and probably in suppression of inflammatory response. Unlike mammals where secondary injury mechanisms lead to apoptotic death of both neurons and glia, here we observe a beneficial role of apoptotic cell death. Injury-induced proliferation, presence of radial glia cells, and their role as progenitor all contribute to cellular replacement and successful neurogenesis after injury in adult zebrafish. Together with cell replacement phenomenon, there is creation of a permissive environment that includes the absence or clearance of myelin debris, presence of Schwann cells, and absence of inflammatory response. *Developmental Dynamics 239:2962–2979, 2010.* © 2010 Wiley-Liss, Inc.

Key words: regeneration; cell death; cell proliferation; spinal cord injury (SCI); neurogenesis; radial glia; zebrafish; Schwann cell; macrophage

Accepted 24 August 2010

INTRODUCTION

Fish and urodele amphibians maintain an extraordinary ability to regenerate a variety of complex body parts including their central nervous system (CNS). In contrast, CNS of mammals including human, have a very limited ability for cellular repair. Any spinal cord injury (SCI) in mammals leads to functional decline because of a progressive pathophysiology affecting cell survival and neurological integrity. The primary mechanical damage is compounded by a complex sequence of cellular events like pronounced inflammatory response by rapid invasion of macrophages/microglia and astrocytes, local loss of neurons and glia, demyelination, axonal degeneration, and formation of fibroglial scar (Balentine, 1978a,b; Blight, 1985; Guth et al., 1999; Popovich et al., 1997; Donnelly and Popovich 2008), which are responsible for development of neuropathology and subsequent loss of functions. The precise mechanisms underlying the expansion of primary injuries are not fully known, although several factors are known to be responsible in secondary degenerative response.

Evidence has also accumulated that demonstrates the existence of a quiescent population of multipotent neural progenitors in the adult mammalian central nervous system contrary to what was previously thought (Morshead et al., 1994; Gage, 2000; Alvarez-Buylla et al., 2002; Song et al., 2002). These cells, upon proper stimulation and with a permissive environment, can even proliferate and differentiate to neurons, which point towards a potential for novel therapeutic strategies to induce regeneration after SCI by generating new neurons. Thus, key requirements for successful regeneration to take place are (1) cellular replacement, i.e., the presence of neurons and glia that could be generated in adequate numbers, (2) significant cell survival after injury and the ability of those neurons to extend axons to the original target, and (3) the axonal remyelination and axonal regrowth. It is a necessary prerequisite to study

Additional Supporting Information may be found in the online version of this article.

[1]Department of Biophysics, Molecular Biology and Bioinformatics, University of Calcutta, Kolkata, India
[2]Chittaranjan National Cancer Research Institute, Kolkata, India

Grant sponsor: DBT, Govt. of India; Grant number: BT/PR5489/AAQ/03/245/2004.

***Correspondence to: Sukla Ghosh, Department of Biophysics, Molecular Biology and Bioinformatics, University of Calcutta, 92, A. P. C Road, Kolkata 700009, India. E-mail: suklagh2010@gmail.com**

DOI 10.1002/dvdy.22438
Published online 8 October 2010 in Wiley Online Library (wileyonlinelibrary.com).

these processes in those species of vertebrates that can regrow their axons and have the capacity to generate new neurons even in adult life.

Adult zebrafish can regrow axons spontaneously after spinal cord transection and are capable of reconnecting their appropriate targets (Becker et al., 1997; Bernhardt, 1999). An unusual feature of fish CNS is that they are neurogenic and they may continue to generate new neurons throughout normal life even in mature uninjured spinal cord (Leonard et al., 1978; Anderson and Waxman, 1983; Waxman and Anderson, 1985). Most of the previous studies on adult neurogenesis and neuronal regeneration in brain are based on different teleost species (Zupanc and Horschke, 1995; Zupanc et al., 2005; Zupanc and Zupanc, 2006). Although zebrafish has emerged as a powerful animal model to study regeneration for various reasons, very little attention has been paid to study spinal cord regeneration in this species. All the previous studies on spinal cord have focused on giving complete transection (Becker et al., 1997, 2005; Reimer et al., 2009) and none of these studies have examined the response to crush, hemisection, or contusion injuries, which are known to be a significant focus of research efforts in mammalian models. Thus, most of the earlier data cannot be compared directly to the results from contemporary studies on mammalian models for SCI.

Evidence from brain injury and SCI in mammalian adult suggests induction of apoptosis, which plays a significant role in secondary degenerative response (Crowe et al., 1995). Injury-induced apoptosis occurs in different neural populations like neurons, astrocytes, oligodendrocytes, and microglia after SCI (Shuman et al., 1996; Liu et al., 1997; Li et al., 1999; Newcomb et al., 1999; Beattie et al., 2000). There are conflicting reports on the absence or presence of injury-induced cell death in fish brain in stages beyond embryogenesis (Fine, 1989; Waxman and Anderson, 1985; Zupanc et al., 1998). So it is imperative to address the issue of cell death in the context of secondary degenerative response in both regeneration-incompetent and regeneration-competent species. It is particularly important to know what happens in regeneration-competent species, where the presence or absence of secondary response has not been confirmed and characterized. In the present report, we have characterized the lesion after injury at the ultrastructural level and also demonstrated a significant level of injury-induced cell proliferation, neurogenesis, and a low level of apoptotic cell death in zebrafish spinal cord after injury, where a comparable mammalian mode of injury, e.g., crush, has been used.

RESULTS

Histology of Uninjured Spinal Cord

Sections from uninjured spinal cord were stained with either hematoxylin/eosin (H&E, Fig. 1A) or luxol fast blue/cresyl violet (Fig. 1J) and trichrome (not shown) to observe the normal structure of uninjured spinal cord. We showed the presence of a very high ratio of white matter compared to grey matter. Presence of ependyma can be seen here, which are two to three cell layers thick (also referred to as ventricular zone) and an ependymal canal runs through the center of the cord. Adjacent to ependyma is a subependymal cell layer that contains neurons (Fig. 1A, J, and J.1).

Time Course Analysis of Regeneration

We have studied the time course of regeneration after giving a crush injury to the adult zebrafish spinal cord. To characterize the injury, we have documented the basic cellular events during regeneration at different time points after injury by using H&E, luxol fast blue, and cresyl violet (Fig. 1), trichrome (Fig. 2) staining, as well as ultrastructural analysis by TEM (Figs.1 and 2). Immediately after injury, there is a loss of the blood-brain barrier, which results in infiltration of blood cells to the injury site, disruption of ependyma, and a substantial loss of tissue, both in white and grey matter (Figs. 1B and 2A). Infiltrating blood cells include macrophages as evidenced by their phagocytic nature (Fig. 2D–G), polymorphonuclear neutrophils (Fig. 2H), monocytes with a horse-shoe-shaped nucleus (Fig. 2I), and red blood cells (RBC; Figs. 1C, 2B), all of which can be seen in 3-day post-injury (dpi) cord. These macrophages are most likely blood-derived since they are located in the close vicinity of the blood vessel (Fig. 2F). A substantially higher number of macrophage infiltrations can be demonstrated at the injured site in 3dpi cord and many macrophages are present around a dying neuron (Fig. 2F), which have a characteristic electron-dense fragmented body in nucleus and retracted cytoplasm (Naganska and Matyja, 2001). At the same time point, damaged axons are shown about to be engulfed by macrophages (Fig. 2E), whereas 10dpi cord shows fewer macrophages at the site of injury (Fig. 2G), although lipophilic inclusions, vacuoles, and some digested residues of myelin debris that were engulfed earlier are present inside the macrophage. Presence of RBC can be predominantly seen close to the injury epicenter in 1-, 3-, and 5dpi cord (Fig. 2A–C) and afterwards the infiltration of RBC decreased considerably (data not shown). Both 1dpi and 3dpi cord showed damaged tissue in grey matter, as disruption of ependyma and compression of the cord is evident (Figs. 1B,C,K, 2A,B). Tissue edema can be observed as a consequence of injury in 3- to 7dpi cord and is reduced afterwards. Loss of white matter (Figs. 1B,C,K, 2A,B), can also be confirmed in injured cord both by luxol fast blue staining (Fig. 1K) and by ultrastructural analysis, which revealed demyelination of axons (Fig. 1O,P) when compared to normal uninjured cord (Fig. 1N). There are accumulations of some cells around the cut ends of ependyma as early as 3dpi, which replace the initial loss of tissue. Cells around the ependymal canal begin to migrate and initiate ependymal sealing at the same time (Fig. 1C, C.1). Accumulation of cells around the injury site continues to occur at 5dpi and 7dpi (Fig. 1D and E, respectively). Progressive ependymal sealing, which is an early regenerative event, can be observed at around 5dpi (Fig. 1D, D.1) when ependymal bulb formation involving ependyma and the ependymal canal is obvious. As both ends of the ependymal bulb join, there is continuation of the ependymal canal, which forms a cavity-like structure in the grey matter of 7dpi (Fig. 1E) and 10dpi cord (Fig. 1F). It is worth mentioning that the size of the cavity-like structure observed at different levels in

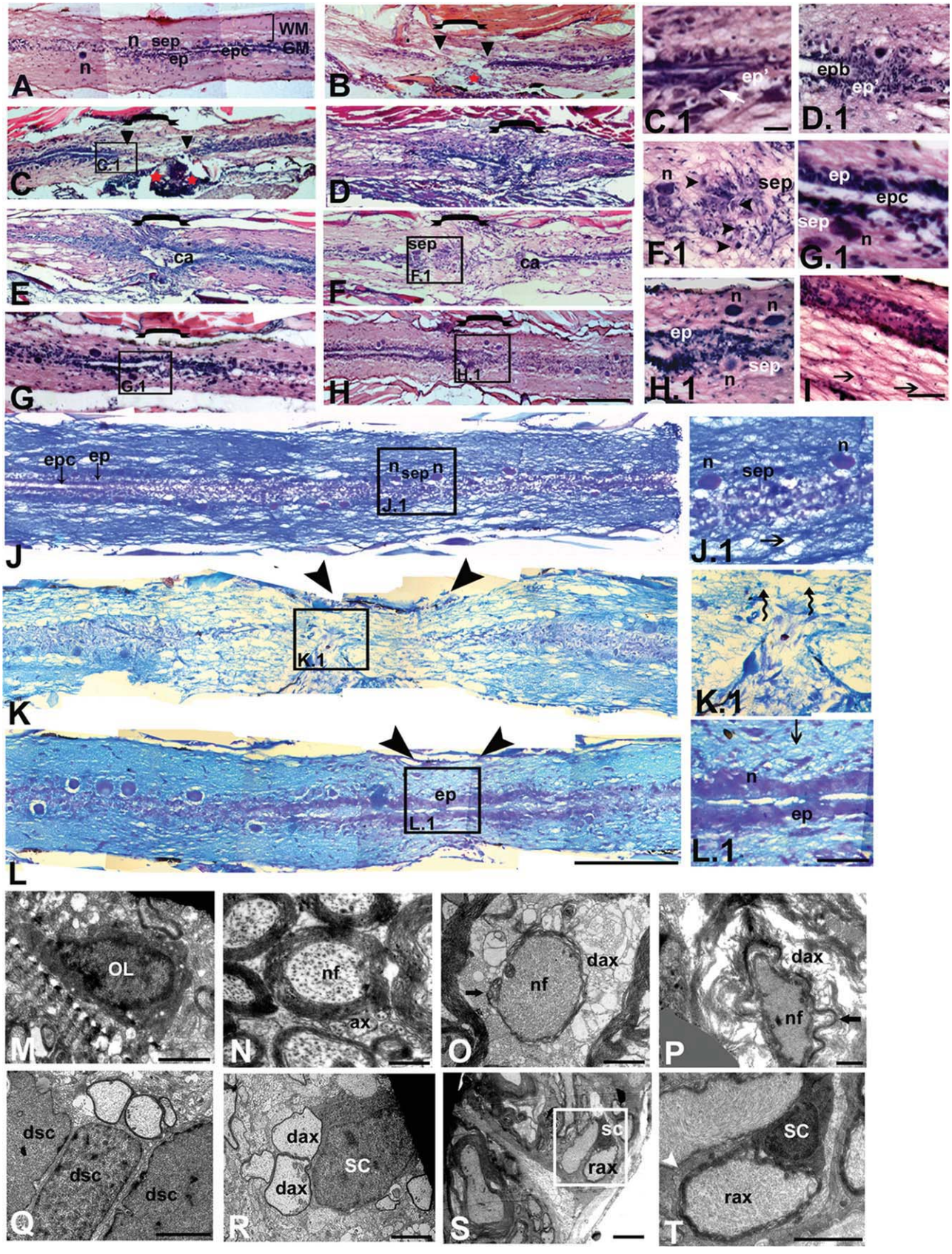
A
n
n
sep
ep
epc
WM
CM
B
C
C.1
C.1
D
D.1
epb
ep
E
ca
F
sep
F.1
ca
F.1
n
sep
G
G.1
G.1
ep
epc
sep
n
H
H.1
H.1
n
n
ep
sep
n
I
J
epc
ep
n
sep
n
J.1
J.1
n
n
sep
K
K.1
K.1
L
ep
L.1
L.1
n
ep
M
OL
N
nf
ax
O
dax
nf
P
dax
nf
Q
dsc
dsc
dsc
R
dax
SC
dax
S
sc
rax
T
SC
rax

Fig. 1.

subsequent sections (data not shown) of 7dpi cord is quite large (1E). The size reduces later at day 10 (Fig. 1F) and further regression can be seen after 15dpi (Fig. 1G and G.1) and at 1 month of injury (Fig. 1H, L) as regeneration progresses. These cavity-like structures are seen only in the grey matter lined by ependymal cells and may not be equivalent to what we see in mammalian SCI, which is a fluid-filled astrocyte-lined cavity present in white matter (Balentine, 1978a,b; Fitch et al., 1999; Renault-Mihara et al., 2008). We also observed newly formed neuronal cell bodies at the injury epicenter, which are small in size at 10dpi cord (Fig. 1F.1) and identity of these cells is further confirmed by using neuronal markers like Hu along with luxol fast blue/cresyl violet staining (see Fig. 6H–K). Both grey matter and white matter regeneration has occurred by day 15 post-injured cord. A regenerated ependyma, subependyma with newly formed neurons in the injury epicenter, and regenerating axons in white matter (Fig. 1G and G.1) can be observed, although white matter volume has not regained the original volume that was present before injury. We followed the regeneration time course for a much longer time period, up to 1 month (Fig. 1H and H.1, I) and 1.5 months post-injury (data not shown). Complete regeneration of ependyma is observed at 1 month post-injured cord with reappearance of lost neurons in the subependyma near the injury epicenter (Fig. 1H and H.1, L and L.1) and axons (Fig. 1L and L.1). Regeneration of white matter took place without formation of a cavity, but even at 1 and 1.5 month(s) after injury, full white matter volume was not regained.

TEM analysis showed presence of oligodendrocytes and myelinated axons with compact myelin sheath and sparsely distributed neurofilament in the axonal body in uninjured cord (Fig. 1M,N). In 3dpi cord, the axons are denuded and typical features of these demyelinated axons are the presence of denser neurofilament within the axonal body (Fig. 1O,P), whereas myelin sheaths are either less compact with irregular shapes or are disintegrating. We observed the presence of Schwann cells around the injured demyelinated axons in 10dpi cord (Fig. 1R), although no Schwann cells are observed in uninjured cord and Schwann cells are seen dividing (Fig. 1Q), which would probably start remyelination (Fig. 1R). Later on, some of these cells are wrapping the axons through basal membrane, suggesting that these cells are indeed involved in the remyelination process after injury (Fig. 1S and T). In regenerated cord 1 month post-injury, the presence of remyelinated axons with thinner myelin sheaths at the injury epicenter can be seen (Fig. 1S,T) when compared to uninjured cord (Fig. 1N).

Analysis of Functional Behavior After SCI

Functional recovery of injured fishes (n=6) has been studied by individually monitoring the swimming behavior of each fish at different time points and they were compared to control uninjured fish. Three different time points of an individual fish have been represented for the sake of simplicity (Fig. 3A–E), although another 5 fishes showed a similar functional recovery (data not shown). We observed loss of swimming behavior primarily because of paralysis of the posterior part of the body beyond the dorsal fin level due to SCI. Very little movement has been recorded at 3dpi (Fig. 3C) compared to uninjured fish. Later on, movements steadily increased beyond the 15-day time point and almost complete functional recovery was documented after 1 month post-injury (Fig. 3E).

Time Course Analysis of Cell Proliferation in the Spinal Cord After Injury and Characterization of Proliferating Cells During Regeneration

We have shown a substantial amount of tissue replacement after crush injury in spinal cord. This led us to study the proliferation pattern using BrdU incorporation (S-phase marker), which detected a spectrum of proliferating cells during this regenerative process. We used a 16-hr BrdU incorporation time length as it represents a saturation label for BrdU uptake in

Fig. 1. Longitudinal sections of normal uninjured (A, J) and injured (B–H and K–L) zebrafish spinal cord after H&E (A–H) and luxol fast blue/cresyl violet staining (J–L). **A, J:** Uninjured spinal cord section shows the presence of white matter (WM), grey matter (GM), neurons (n) in the subependyma (sep), and ependyma (ep) with ependymal canal (epc). **J.1:** The higher magnification of J shows an axon (→) in white matter and neurons (n) in the subependyma (sep). **B:** 1dpi-section of spinal cord showing loss of both white and grey matter, infiltration of blood cells (red *), and disrupted ependyma (▼▼) at the injury epicenter ([bracket]). **C, K:** 3dpi cord shows blood clot at the site of injury (**) and same section at higher magnification (**C.1**) showing initiation of sealing of ependymal canal (ep′) and migrating ependymal cell (white arrow). Another section of 3dpi cord (K) showing severed ependyma, axonal loss (spiral arrow) and neuronal loss at the injury epicenter (double arrowheads). **K.1:** Higher magnification of K. **D:** 5dpi cord reveals accumulation of cells at epicenter and tissue edema. Another 5dpi cord at higher magnification (**D.1**) shows complete sealing of ependyma (ep′) and formation of ependymal bulb (epb). **E:** Section of 7dpi cord reveals accumulation of cells at the injury epicenter, swelling of tissue, and also the presence of a continuous cavity like structure (ca) surrounded by ependymal cells. **F:** 10dpi cord showing the presence of a smaller cavity (ca) -like structure continuous with regenerating ependymal canal. **F.1:** Same cord at higher magnification, showing the presence of many newly formed cells (▶) and a mature neuron (n) in the injury epicenter. **G:** Representative section of 15dpi cord reveals a normal regenerated ependyma with complete absence of a cavity-like structure and partially regenerated white matter. **G.1:** Higher magnification of the same section shows well-formed ependyma (ep) with an ependymal canal (epc) and regenerated neuron (n) in subependyma (sep). **H, L:** One-month regenerated cord shows both grey and white matter regeneration and both neurons (n) and axons (→) are clearly visible at the injury epicenter at higher magnification (**H.1, I**). Another section (**L**) showing regeneration of both white matter and grey matter at the injury epicenter and the same cord at higher magnification (**L.1**) showing small neuronal cell bodies (n), reconnected axons (↓), and compact ependyma (ep). **M, N:** Oligodendrocyte (OL) and myelinated axon (ax), with sparsely distributed neurofilaments (nf) within the axonal body in uninjured cord, respectively. **O–P:** Representative picture of demyelinating axons (dax) at the injury epicenter of 3dpi cord showing denuded axon (bold arrow) and axonal body with dense neurofilaments (nf). **Q,R:** 10dpi cord showing dividing Schwann cells (dsc) and Schwann cells (SC) associated with demyelinated axons (dax) at the injury epicenter, respectively. **S:** Remyelinating axon (rax) with Schwann cells (SC) in regenerating cord 1 month post-injury. **T:** Higher magnification of indicated area in S showing the basal membrane of Schwann cells (white arrowhead) around the remyelinating axon (rax). Scale bar = 400 μm (A–H), 20 μm (C.1), 40 μm (D.1–I), 200 μm (J–L), 60 μm (J.1–L.1), 2 μm (M–T).

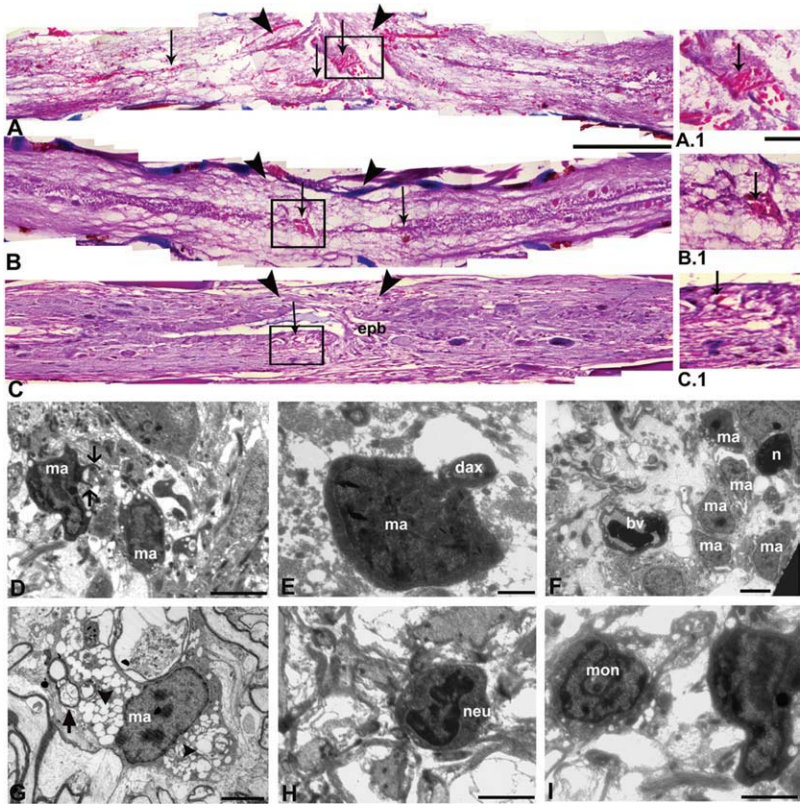

Fig. 2.

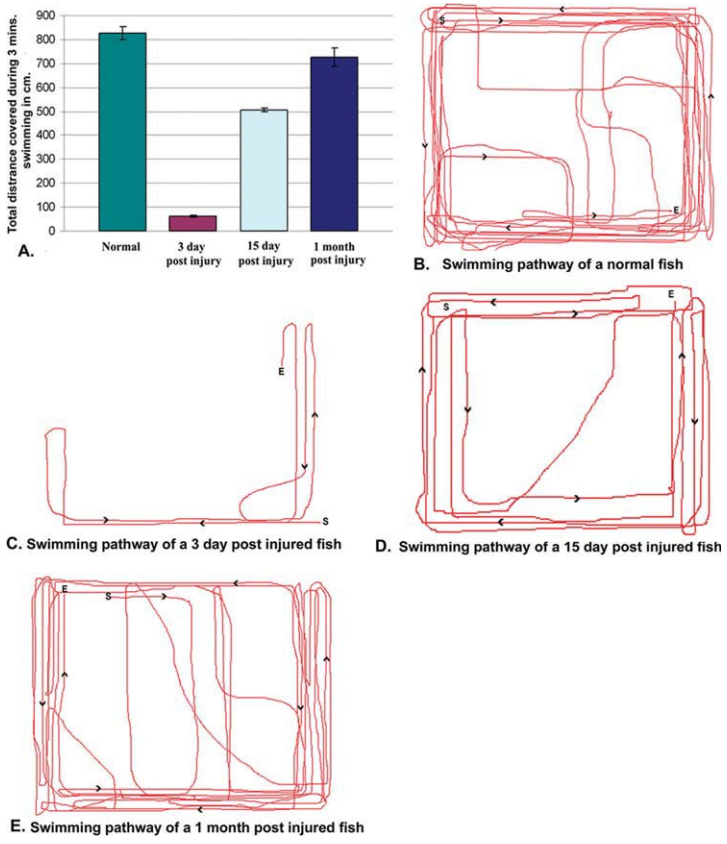

Fig. 3.

zebrafish CNS. A previous report showed that a pulse-label BrdU uptake between 12–16 hr represents all cycling cells went through at least one S phase during incubation (Mueller and Wullimann, 2002). The data of BrdU incorporation in uninjured and injured spinal cord tissues at different time points (3dpi to15dpi) are represented in Table 1 and Figure 4A–G. In order to show that cells at S-phase are indeed going through mitosis, we have used another proliferation marker, phosphohistone 3 (H3P) (Fig. 4H,I).

BrdU incorporation was recorded in adult uninjured cord both in white matter and grey matter. Many $BrdU^+$ cells around the ependymal canal can be seen and the percentage of positive cells in grey matter is higher than

Fig. 2. Trichrome staining (A-C) and ultrastructural analysis (D-I) of injured zebrafish spinal cord. **A:** 1dpi cord shows infiltration of large number of RBC (↓) both at the injury epicenter (double arrowheads) and also towards the normal part of the cord. **B:** A 3dpi cord showing less number of infiltrating R.B.C. **C:** A 5dpi cord shows presence of very few blood cells and the appearance of ependymal bulb (epb) at the injury epicenter. **A.1, B.1, C.1:** Higher magnification representation of A, B, and C, respectively, showing the presence of blood cells at the injury epicenter. **D–G**: Presence of macrophages (ma) at the injury epicenter in 3dpi (D–F) and 10dpi (G) cord. **D, E:** Macrophage (ma) with a typical phagocytic process (↑) and in close proximity to a demyelinating axon (dax), respectively. **F:** A dying neuron (n) with condensed nuclear matter surrounded by infiltrated macrophages (ma) and a blood vessel (bv) nearby. **G:** Macrophage (ma) with many lipophillic vacuoles (▶) and phagocytosed myelin debris (thick arrow). **H, I:** The presence of neutrophils (neu) and monocytes (mon), respectively, in 3dpi cord. Scale bar = 250 μm (A–C), 50 μm (A.1–C.1), 5 μm (D, F), 2 μm (H, I), 1 μm (E, G).

Fig. 3. Recovery of functional swimming behavior after crush injury in spinal cord of zebrafish. **A:** Quantification of swimming distance shows that the 3dpi fish covered much less distance during swimming compared to normal fish, whereas a substantial gain in function can be observed in 15dpi and 1-month post-injured fish. Error bar indicates values Mean ± SEM. **B–E:** The line diagrams represent swimming distance and route covered by a normal uninjured, 3dpi, 15dpi and 1-month post-injured fish, respectively, and indicate the significant recovery in function at 1 month after SCI. S, starting point; E, end point; arrows, direction of swimming pathway.

TABLE 1. Time Course Analysis of BrdU Incorporation in Uninjured and Injured Spinal Cord[a]

A. Cell proliferation in uninjured zebrafish spinal cord (total length of tissue sectioned = 4 mm including injury epicenter, thickness of section = 7 μm) after 16-hr BrdU incorporation.

No. of sections counted	Brdu+ cells in grey matter/section	Brdu+ cells in white matter/section
74 (n=6)	3.95 ± 0.286 *	5.89 ± 0.244 *

B. Cell proliferation in injured zebrafish spinal cord (total length of tissue sectioned = 4 mm including injury epicenter, thickness of section = 7 μm) after 16-hr BrdU incorporation.

Time point after SCI (days)	No. of sections counted in LS	Brdu+ cells/section in the injury epicenter (grey matter). Approx. 300 μm	Brdu+ cells/section in the injury epicenter (white matter). Approx. 300 μm	Brdu+ cells/section in adjacent normal part (grey matter). Approx. 1,800 μm both rostral and caudal	Brdu+ cells/section in adjacent normal part (white matter). Approx. 1,800 μm both rostral and caudal
3 day	79 (n=6)	4.02 ± 0.142 **	3.97 ± 0.259 **	20.05 ± 0.563	7.86 ± 0.326
7 day	86 (n=6)	14.96 ± 0.362*,**	11.13 ± 0.402*,**	28.02 ± 0.522*	12.96 ± 0.239*
10 day	76 (n=6)	6.86 ± 0.158	6.03 ± 0.209	11.65 ± 0.486	10.56 ± 0.365
15 day	72 (n=6)	3.76 ± 0.128	3.25 ± 0.153	9.86 ± 0.518	7.08 ± 0.324

[a]Values are represented as Mean ± SEM
*$P<0.001$, between total count of 7 day post injured cord versus uninjured cord.
**$P<0.01$, between total count of injury epicenter of 7 day versus 3 day.

that in the white matter (Fig. 4A,B). Since the volume of total white matter tissue is higher than that of total grey matter, the total number of $BrdU^+$ cells in white matter is higher than that in grey matter (Table 1A). Here grey matter represents both the ventricular zone and subependyma and proliferation involves cells from both these regions, although the rate of proliferation in the ventricular zone is much higher than in the subependymal zone (Fig. 4B).

When we compare the level of BrdU incorporation in different regions of the injured cord at different time points after injury (Table 1B), we observe an increased level of incorporation after 3dpi (Fig. 4C), compared to the uninjured cord (Fig. 4A,B). An almost equal level of BrdU incorporation is represented in white and grey matter in the epicenter of injury. Total BrdU incorporation shown here in the injury epicenter is less than that in the adjacent part (which represents a larger area), but considering the fact that the epicenter represents a smaller area compared to the adjacent part, density of $BrdU^+$ cells in the injury epicenter is still higher (Table 1B and Fig. 4C). The number of BrdU incorporation still increases significantly both in the injury epicenter and the adjacent part in 7dpi cord (Table 1B and Fig. 4D) when compared to 3dpi cord and uninjured cord. The number of the $BrdU^+$ cells increases at the injury epicenter both in grey and white matter (Fig. 4D and Table 1B). Similar to previous time points, total incorporation in 7dpi cord is higher in the adjacent zone compared to the injury epicenter since the adjacent part includes wider areas than the epicenter, whereas the actual density of the $BrdU^+$ cells is much higher than 3dpi cord higher at the injury epicenter (Fig. 4D and Table 1B). This increase in number of $BrdU^+$ cells at the injury epicenter in 7dpi cord may be indicative of migration of cells from the adjacent zone to the injury epicenter (Fig. 4C, D, and Table 1B). We have analyzed H3P staining in regenerating cord. The 7dpi cord (Fig. 4H,I) showed many $H3P^+$ cells at the injury site as well as at the adjacent part compared to uninjured cord (data not shown) after giving a single pulse of BrdU for 16-hr $BrdU^+$ cells in uninjured cord include both slow-dividing cells with intense labeling as well as fast-dividing cells with weak labeling (Fig. 4K). The presence of slow-dividing cells can be confirmed further in 7dpi cord where we used 48-hr BrdU pulse continuously after giving injury and chased up to 7 days. The pulse-chased 7dpi cord shows the presence of slow-dividing $BrdU^+$ cells (Fig. 4L), which have entered into S-phase during the first 48 hr after injury and they are still in S-phase after 7 days.

In all the time points after injury, the two regions, namely the injury epicenter and the adjacent part, showed that the total level of incorporation is always higher around the grey matter compared to the white matter, unlike uninjured cord. BrdU incorporation in 10dpi cord (Fig. 4E and Table 1B) was also studied where the level is lower than 7dpi cord. The actual density of BrdU-incorporated cells in the injury epicenter could be still higher than the region away from the injury site as observed in another two time points. The rate of BrdU incorporation slows down further in 15dpi cord in both these regions (Fig. 4F and Table 1B).

Radial Glia as Proliferating Precursors

We observe that in the adult uninjured cord, radial glial cells are present

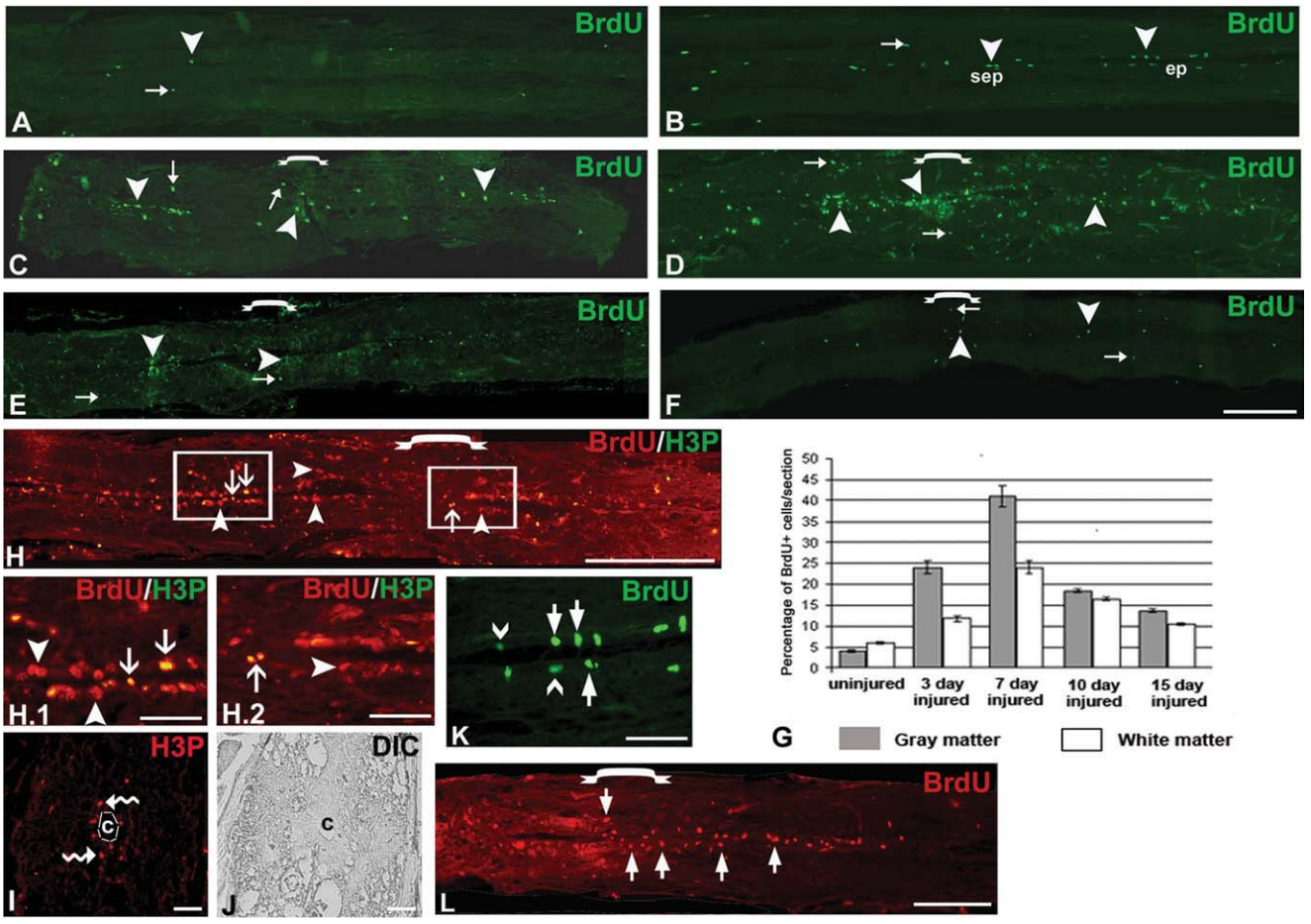

Fig. 4. Time course analysis of injury-induced cell proliferation represented after BrdU incorporation and H3P staining in uninjured and injured spinal cord. **A, B:** Uninjured cord shows $BrdU^+$ cells are present both in grey matter (▼) and white matter (→) but mostly in ependyma (ep). **C:** 3dpi cord shows a large increase in $BrdU^+$ cells in both grey (▼) and white (→) matter. **D:** A section of 7dpi cord shows a very significant increase in number of $BrdU^+$ cells in both grey (▼) and white matter (→), and increased numbers of cells are present at the injury epicenter ([down bracket]) compared to 3dpi cord. **E:** A 10dpi cord shows incorporation in both white matter (→) and grey matter (▼) but a considerable decrease in number of $BrdU^+$ cells compared to 7dpi cord. **F:** A 15dpi cord section shows fewer $BrdU^+$ cells in grey (▼) and white matter (→) compared to the 10dpi cord and the number is still higher than in the uninjured cord. **G:** Quantitative representation of $BrdU^+$ cells in both grey and white matter of uninjured and injured cord at different time points. **H:** A 7dpi cord section shows $BrdU^+$ cells (▼) and many of these are colocalized with H3P (↓) in both the injury epicenter ([down-bracket]) and adjacent part. **H.1, H.2:** Same 7dpi cord as in H showing adjacent area and injury epicenter, respectively, at high magnification. **I, J:** Another representative cross-section of 7dpi cord showing distribution of $H3P^+$ cells (⇝) around the central canal (c) and DIC of same section. **K:** Ependyma of uninjured cord showing both slow-dividing (thick arrow) and fast-dividing (∨) cells. **L:** Section of 7dpi cord showing $BrdU^+$ slow-dividing cells (thick arrow) after 48-hr continuous BrdU pulse. Scale bar = 400 μm (A–H), 20 μm (H.1–K), 200 μm (L).

around the ependymal canal and are strongly GFAP positive. Approximately 6.9% of the total populations are radial glia in an uninjured cord. All the cells around the ependymal canal are not radial glia as these are $GFAP^-/DAPI^+$ cells (Fig. 5A). Among the radial glia some (1.4% of total cell populations) are $BrdU^+$ even in uninjured cord (Fig. 5B). Most of the $BrdU^+$ radial glia are slow, although a small population of slow-dividing cells is not radial glia (Fig. 5D.1, E). Immediately after injury, 3dpi cord showed a down-regulation of GFAP expression at the injury epicenter (Fig. 5H) compared to uninjured cord (Fig. 5D) and the immediate adjacent area of the injury epicenter was weakly stained. In later time points, there was a reappearance of $GFAP^+$ cells with a moderate increase in the level of expression in day 7 (Fig. 5I), followed by a higher level in day 15 (Fig. 5J), and a near to normal level of expression in 1-month post-injured cord (data not shown).

We have also identified three different populations of cells, $BrdU^+/GFAP^+$, $BrdU^+/GFAP^-$, and $BrdU^-/GFAP^+$, both in uninjured cord and in injured cord but their percentage varies in injured cord (Fig. 5D–J, a–d). The pie chart represents the relative percentage of colocalized cells ($BrdU^+/GFAP^+$, $BrdU^+/GFAP^-$, $BrdU^-/GFAP^+$, and $DAPI^+$) in uninjured and injured cord. Numbers of different population of cells are counted in the sections from two spinal cords at each time point. Data on the counts of different populations are mentioned in Supplemental Figure S1 (which is available online). It has been observed that approximately 1.2 and 1.6% cells are both $BrdU^+/GFAP^+$ in 3dpi (Fig. 5H, H.1, and b) and 7dpi (Fig. 5I, I.1, I.2, c) cord, respectively, which are more or less similar to uninjured cord, indicating that this particular population of cells is probably being maintained in both uninjured and injured cord

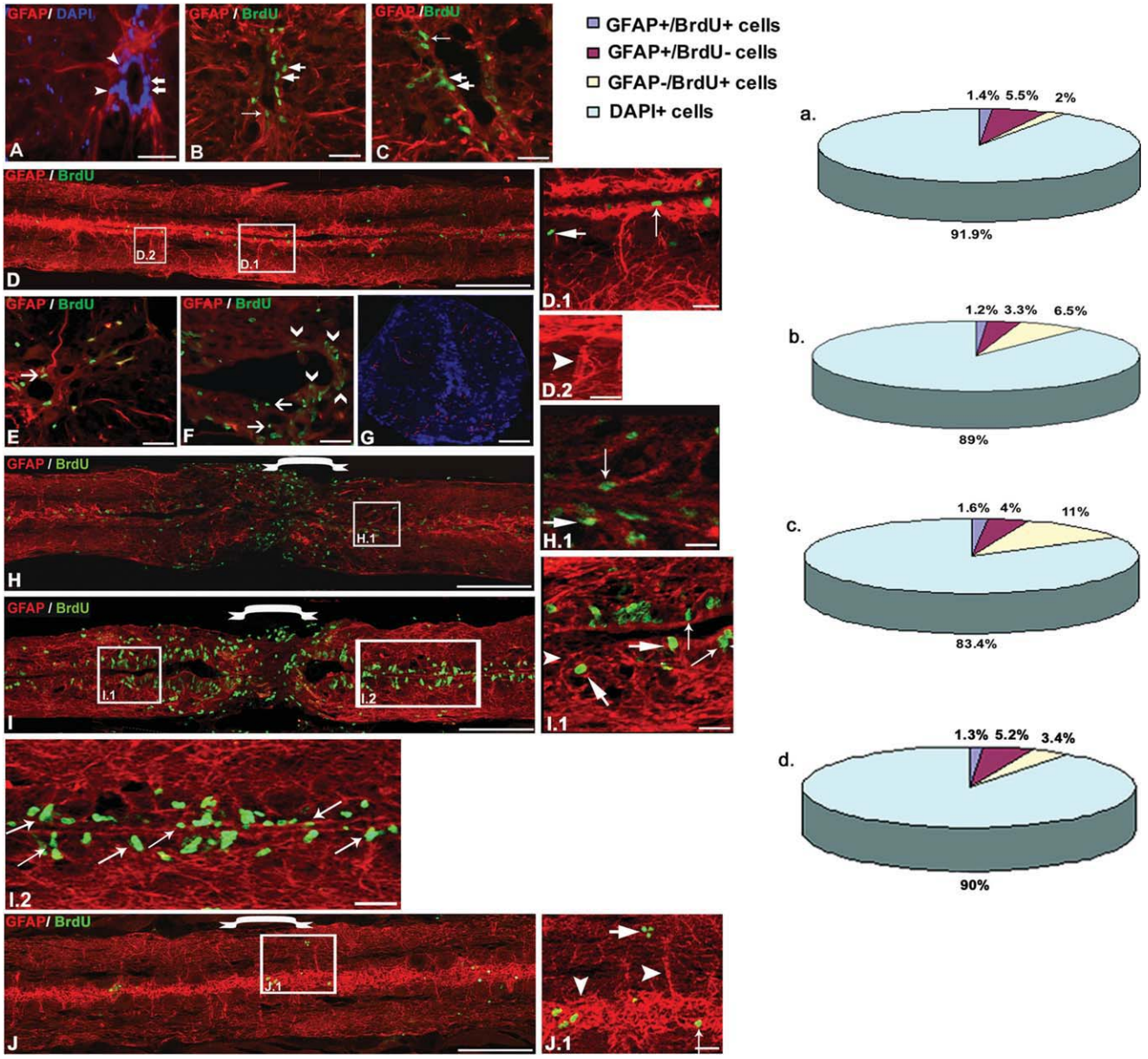

Fig. 5. Immunohistochemical staining of GFAP and BrdU in zebrafish uninjured (A,B, D,E, D.1, and D.2) and injured (C, F, H–J, H.1, I.1, and J.1) spinal cord. **A, B:** Uninjured cord section showing that a percentage of DAPI$^+$ cells are GFAP$^+$ radial glia (arrowhead) and the presence of BrdU$^+$ cells (thick arrow) around the central canal; some colocalize with GFAP (→). **C:** 7dpi cord section shows a greater number of BrdU$^+$ cells around the central canal than normal; a few colocalized with GFAP (→). **D:** Uninjured cord showing high GFAP expression and the presence of few BrdU$^+$ cells. Same cord at a higher magnification showing different radial glial population, GFAP$^+$/BrdU$^+$ (↑) and GFAP$^-$/BrdU$^+$ (thick arrow) cells (**D.1**) and GFAP$^+$/BrdU$^-$ cells (▼) (**D.2**), respectively. **E:** Ependyma of uninjured cord showing many more slow-dividing cells (→), some of which are radial glia and a few fast-dividing cell. **F:** 7dpi cord representing many BrdU$^+$, fast-dividing cells that are GFAP$^-$ (▽) and fewer slow-dividing cells (→) around ependyma. **G:** Control section stained without GFAP primary antibody. **H:** 3dpi cord, showing proliferating BrdU$^+$ cells; only some are GFAP$^+$. Also shown is a loss of GFAP expression at the injury epicenter ([down-bracket]) and at an immediately adjacent part of the cord. **H.1:** Same cord as in H at higher magnification showing both GFAP$^+$/BrdU$^+$ (↑) and GFAP$^-$/BrdU$^+$ (thick arrow) cells. **I:** 7dpi cord showing high proliferation, a low level of GFAP expression at the injury epicenter, and little higher level of GFAP expression at the immediate adjacent area. **I.1:** Same cord at higher magnification shows presence of GFAP$^+$/BrdU$^+$ (↑), GFAP$^-$/BrdU$^+$ (thick arrow) and GFAP$^+$/ BrdU$^-$ (▼) cell populations. **I.2:** Same cord shows the presence of many GFAP$^+$/BrdU$^+$ (↑) cells. **J:** Fifteen-day regenerated cord shows a reduced BrdU incorporation but a high level of GFAP expression in both the uninjured part and the injury epicenter. **J.1:** Same section at higher magnification also represents three populations. **a–d:** The pie chart represents the percentage of three cell populations and DAPI$^+$ cells in adult uninjured (a), 3dpi (b), 7dpi (c), and 15dpi (d) cord, respectively. Scale bar = 250 μm (D and H–J), 20 μm (A–C, E–G, D.1–J.1).

continuously. Most importantly, the population of BrdU$^+$/GFAP$^+$ cells that are represented both in 7dpi cord (Fig. 5I.1) and uninjured cord (Fig. 5D.1) are predominantly slow. There is an increase in both slow- and fast-dividing cells in 7 dpi cord, the relative proportion of fast-dividing BrdU$^+$ cells being much higher and mostly GFAP negative (Fig. 5F).

After injury there is a rapid increase in the percentage of another population of cells, BrdU$^+$/GFAP$^-$, in both 3dpi (8.5% of the total cells counted) and in 7dpi cord (11%) (Fig.

5H,I, b,c). However, at a later time point like 15dpi cord, $BrdU^+/GFAP^-$ cells are significantly decreased to 3.4% (Fig. 5J, d). This is suggestive of the presence of a different population of proliferating precursors namely $BrdU^+/GFAP^+$ cells, which are radial glia but their percentage remains the same before and after injury, whereas the second population of $BrdU^+/GFAP^-$ cells are most important and exist during regeneration in a much higher proportion.

A third population of cells, $BrdU^-/GFAP^+$, is also present both in uninjured (Fig. 5D.2) and injured cord (Fig. 5I.1, J.1). There is a decrease in $BrdU^-/GFAP^+$ cell numbers after injury, both in 3 and 7dpi cord (approximately 3–4% of the total population) compared to uninjured cord (5.5% of total population). They are non-dividing radial glia and their population has decreased following injury.

Neurogenesis: Expression of Neuronal Markers

We have used different markers to identify different neuronal populations present in uninjured and regenerating cord. Immunohistochemical staining with beta III tubulin showed the presence of different types of neurons. These include more dorsally placed sensory neurons, a variety of medially placed interneurons, and more ventrally placed motor neurons in uninjured cord (Fig. 6A; Appel and Chitnis, 2002; Wilson et al., 2002). There is extensive loss of neurons in 3dpi cord (Fig. 6B) and replacement of neurons at the injury epicenter 1 month after regeneration as observed by beta III tubulin staining (Fig. 6C). We have confirmed the presence of newly generated neurons in subependyma with another neuronal marker-Hu in 10dpi cord (Fig. 6H–J). Both uninjured (Fig. 6D–G) and injured cord (Fig. 6H–K) showed the presence of neurons in the subependyma, as confirmed by luxol fast blue and cresyl violet staining (Fig. 6G and K) and their relative position across the dorso-ventral axis (Fig. 6D,E and H,I). Newly formed neurons are present in all three positions like dorsal, medial, and ventral, similar to uninjured cord. Distinctive morphological characteristics of sensory, interneuron, and motor neurons cannot be distinguished in injured cord, as these are small and similar in size and not yet fully differentiated. Since beta III tubulin is expressed only in mature post-mitotic neurons, we have used markers like Hu and NeuroD to understand neuronal differentiation during regeneration. Both Hu protein, which is known to be expressed very early during neuronal differentiation in zebrafish (Kim et al., 1996; Park et al., 2000), and NeuroD, a marker for neuronally determined cells (Korzh et al., 1998), were used to show the nature and time of appearance of newly formed neurons in regenerating cord. Both uninjured and injured cords do express Hu protein (Fig. 6D–F, 6H–J and Fig. 7A–D). Staining with Hu antibody in the 7dpi cord, when we see highest rate of proliferation showed positive cells both in the injury epicenter as well as in the normal part of the cord (Fig. 7D; Supp. Fig. S2P–U). $Hu^+/BrdU^+$ cells can be localized both in the ependymal and subependymal zone with a higher percentage in the subependymal zone (Fig. 7D, D.1), whereas in the uninjured part of the same cord Hu-positive cells are present only in the subependymal zone (Fig. 7D). Unusual subpial localization of $Hu^+/BrdU^+$ cells is also seen in injured cord (Fig. 7D.3). There are many $Hu^+/BrdU^+$ cells in the injury epicenter and in the immediate adjacent part, which are small with little condensed cytoplasm (Fig. 7D.1, D.4, D.5; Supp. Fig. S2R and X, respectively). We observed that among the $Hu^+/BrdU^+$ cells many are fast dividing and few are slow dividing (Fig. 7D.5a–d). Some cells that are $Hu^+/BrdU^-$ can also be recognized in both the injury epicenter (Fig. 7D.1, Supp. Fig. S2R) and immediate adjacent part (Fig. 7D.4, Supp. Fig. S2X), because Hu^+ cells represent a newly formed progeny of neuronal lineage that have just exited from cell cycle. We have also analyzed NeuroD expression at different time points. There is no expression of this particular protein at 7dpi cord (data not shown) although these $NeuroD^-$ cells are Hu^+ and are present in both the injury epicenter and the normal part of the cord. The first appearance of $NeuroD^+$ cells in the injury epicenter can be seen at 10dpi cord and some are co-localized with Hu (Fig. 7B, B.1; Supp. Fig. S2D–F). We also confirm this result with histological analysis of 10dpi cord (Figs. 1F.1, 6K) where we see the reappearance of the neuronal cell body at the injury epicenter. The expression of NeuroD is transient and cannot be seen in 15dpi cord. Co-localized expression of NeuroD and Hu protein revealed the presence of the newly specified neurons, which are still smaller in size in the injury epicenter at 10dpi cord, although some showed projections (Fig. 7B.1). The newly specified neurons with $Hu^+/NeuroD^+$ expression can also be seen in the immediate adjacent part of the injury epicenter, with an obviously smaller number than $Hu^+/NeuroD^-$ cells (Fig. 7B.2, Supp. Fig. S2G–I). Ultrastructure analysis of 10dpi cord also confirmed the presence of dividing neuronal progenitors (Fig. 7E) and 1-month regenerates showed the presence of both mature motor neurons and newly generated neurons with little cytoplasm containing new but fewer organelles (Fig. 7F–H).

Cell Death in Spinal Cord Injury

We have performed TUNEL and caspase-3 analysis to investigate the role of apoptotic cell death after SCI in zebrafish (Fig. 8). TUNEL analysis at different time points revealed that apoptotic cell death was occurring at the injury site, where the first appearance of TUNEL-positive cells was evident at around 6 hr post-injury (Fig. 8A). At 1dpi, many cells are positive compared to 6 hr post-injured cord, indicative of cell death in higher numbers (Fig. 8B). The number of apoptotic cells decreases at 3dpi cord (Fig. 8C) and is almost absent in 7dpi cord (data not shown), when compared to 1dpi cord (Fig. 8B). Morphological observation of the labeled cells revealed nuclear fragmentation as evident in many cells (Fig. 8B.1).

We have confirmed TUNEL results with another apoptotic cell death marker caspase-3, which is known to be expressed during neuronal and glial loss after SCI in mammals (Citron et al., 2000; Takagi et al., 2003). Although a weak expression of caspase-3 starts as early as 6 hr and is present at 12 hr post-injury (data not shown), the highest level can be seen in 1dpi cord with higher intensity and cell numbers than at the previous time points (Fig. 8D–E). Afterwards

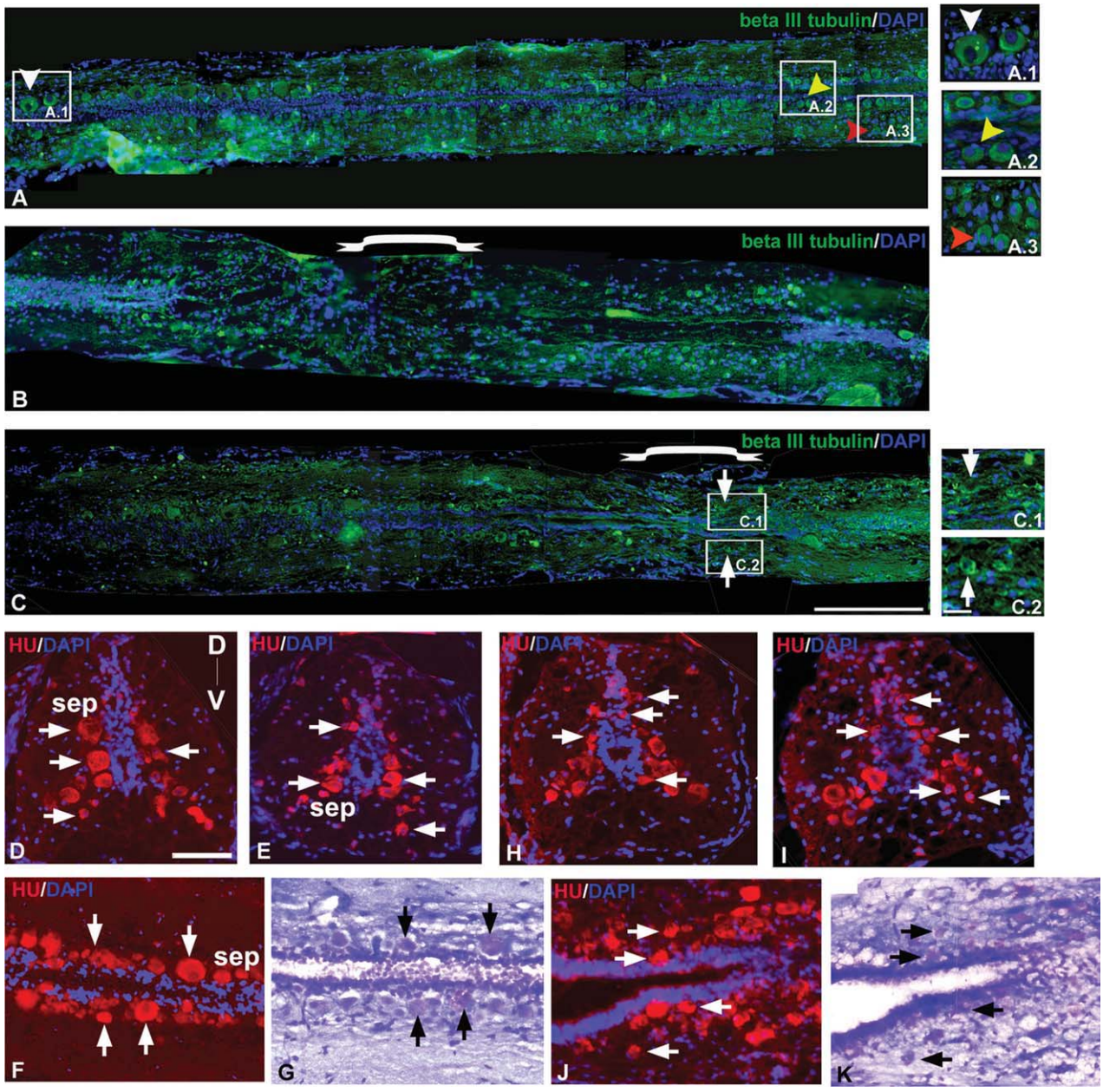

Fig. 6. Immunohistochemical staining of β-III tubulin (A–C), Hu (D–F and H–J), and counter-staining of Luxol fast blue/Cresyl violet (G and K) in zebrafish uninjured (A, D–G) and injured spinal cord (B,C, and H–K). **A:** Section of uninjured cord shows the spatial distribution of different types of neurons sensory neurons (white ▼), interneurons close to ependyma (yellow ▼), and motorneurons (red ▼). **A.1, A.2, A.3:** Higher magnification of indicated areas of A showing different types of neurons. **B:** 3dpi cord section showing the loss of mature neurons at the injury epicenter. **C:** One month post-injured cord section showing regenerated neurons at the injury epicenter. **C.1, C.2:** Higher magnification of indicated areas in C, where formation of new neurons (thick arrow) both at the dorsal and ventral sides can be seen. **D–F:** Sections of uninjured cord showing the distribution of Hu^+ neurons (thick arrow) in the subependyma (sep) along the D-V axis. **G:** Luxol fast blue/Cresyl violet staining of F. **H–J:** Sections from 10dpi cord showing the presence of Hu^+ newly formed neurons (thick arrow) in different locations along the D-V axis. **K:** Staining of the same section in J with Luxol fast blue/Cresyl violet. Scale bar = 250 μm (A–C), 50 μm (A.1–A.3, C.1,C.2, D–K).

the level of expression and number of caspase-3-positive cells decline in 3dpi cord (data not shown). Immunochemistry data were confirmed further by ELISA analysis (Fig. 8I). Ultrastructural analysis revealed apoptotic cell death in neurons (Fig. 8F and G) where condensed nuclear matter with an apoptotic body can be recognized. Mitochondria-associated apoptotic cell death can also be observed in 3dpi cord as we see dying mitochondria in the cytoplasm of an apoptotic neuron (Fig. 8H).

DISCUSSION

Cellular Response to Injury

We have characterized the cellular events to understand (1) the extent of similarity or difference in the cellular responses to trauma in zebrafish cord

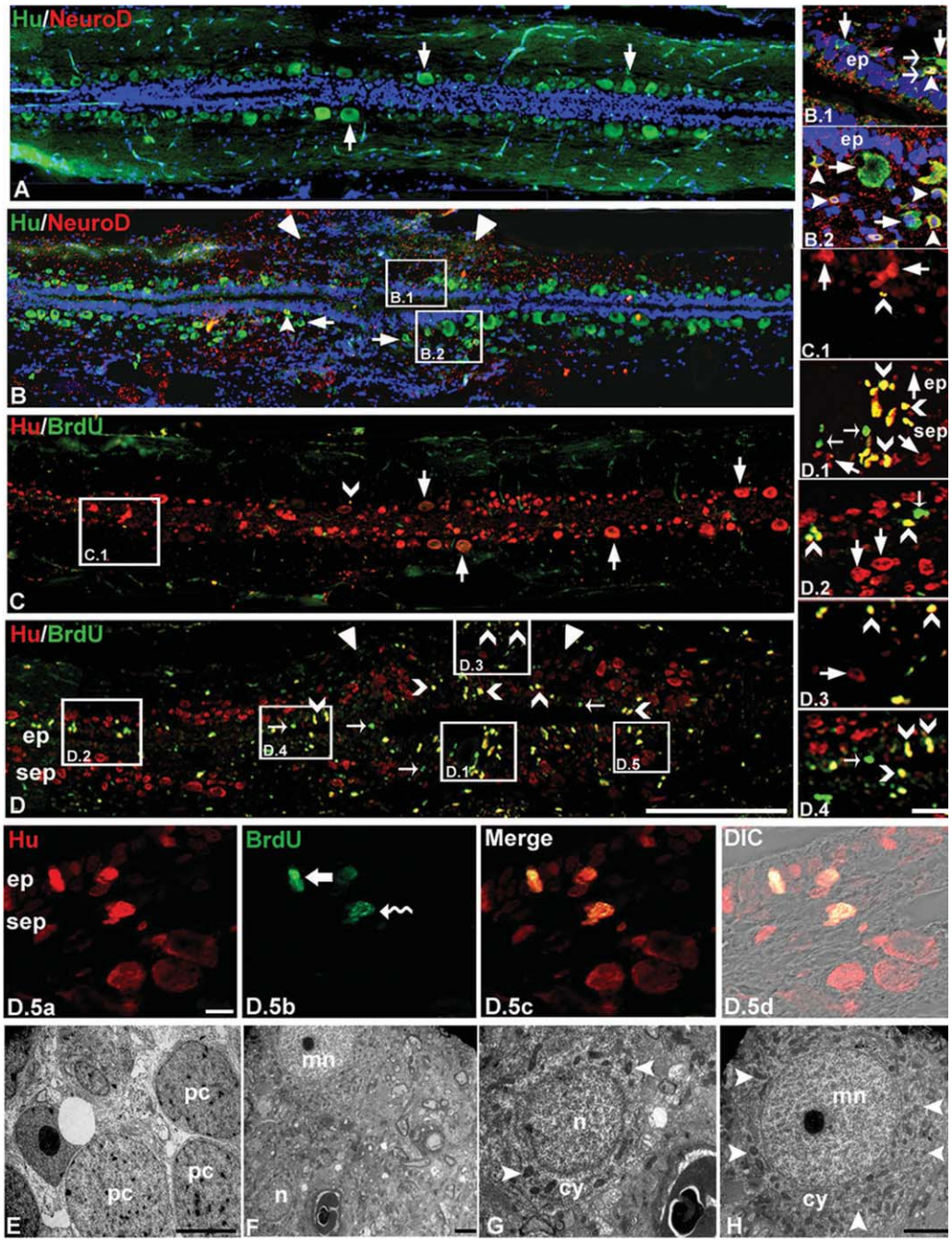

Fig. 7. Immunohistochemical localization of Hu, NeuroD, and BrdU (A–D) and ultrastructural analysis (E–H) in zebrafish spinal cord. **A:** Uninjured spinal cord shows the presence of many Hu^+ cells (thick arrow) in subependyma, which are $NeuroD^-$. **B:** The 10dpi cord section shows Hu^+ cells (thick arrow) at the injured site (▼▼) and a few of these are $NeuroD^+$ (▲). **B.1, B.2:** Higher magnification of indicated areas in B showing both populations of cells in the injury epicenter and the immediate adjacent part, respectively. Note that newly generated neurons extend projections (side arrow). **C:** Uninjured cord showing many subependymal Hu^+ cells (thick arrow) and very few of them are $BrdU^+$ (∨). **C.1:** At higher magnification, the same section as in C showing both $Hu^+/BrdU^-$ cells (thick arrow) and $Hu^+/BrdU^+$ cell (∨). **D:** The 7dpi cord section shows only $BrdU^+$ cells (→) both at the injury epicenter and in the immediate adjacent part of the epicenter. In both these regions, the number of $Hu^+/BrdU^+$ cells (∨) are higher than the normal uninjured cord and are also present close to the pial membrane at the injured site (▼▼). **D.1–D.4**: Same as D at higher magnification showing the presence of $Hu^+/BrdU^+$ (∨), $Hu^+/BrdU^-$ thick arrow), and $Hu^-/BrdU^+$ (thin arrow) cells in the injury epicenter (**D.1**), adjacent normal part (**D.2**), subpial location (**D.3**), and the immediate adjacent part of epicenter (**D.4**) respectively. **D.5:** Represent the presence of both slow (bold arrow) and fast (⇝) population (**D.5b**) of Hu^+ cells in both ependyma (ep) and subependyma (sep) (**D.5a**) and their respective merge (**D.5c**) and DIC (**D.5d**). **E:** 10dpi cord showing dividing neuronal progenitor cells (pc) at the injury site. **F:** One-month post-injured cord shows the presence of both newly formed neuron (n) and specified motor neuron (mn). **G:** Higher magnification picture of newly formed neuron (n) with a small cytoplasmic area (cy) and a few cytoplasmic organelles (white arrowhead). **H:** Higher magnification picture of specified motor neuron with a large volume of cytoplasm and many cytoplasmic organelles (white arrowhead). Scale bar = 200 μm (A–D), 20 μm (B.1–D.3), 10 μm (D.4), 2 μm (E–H).

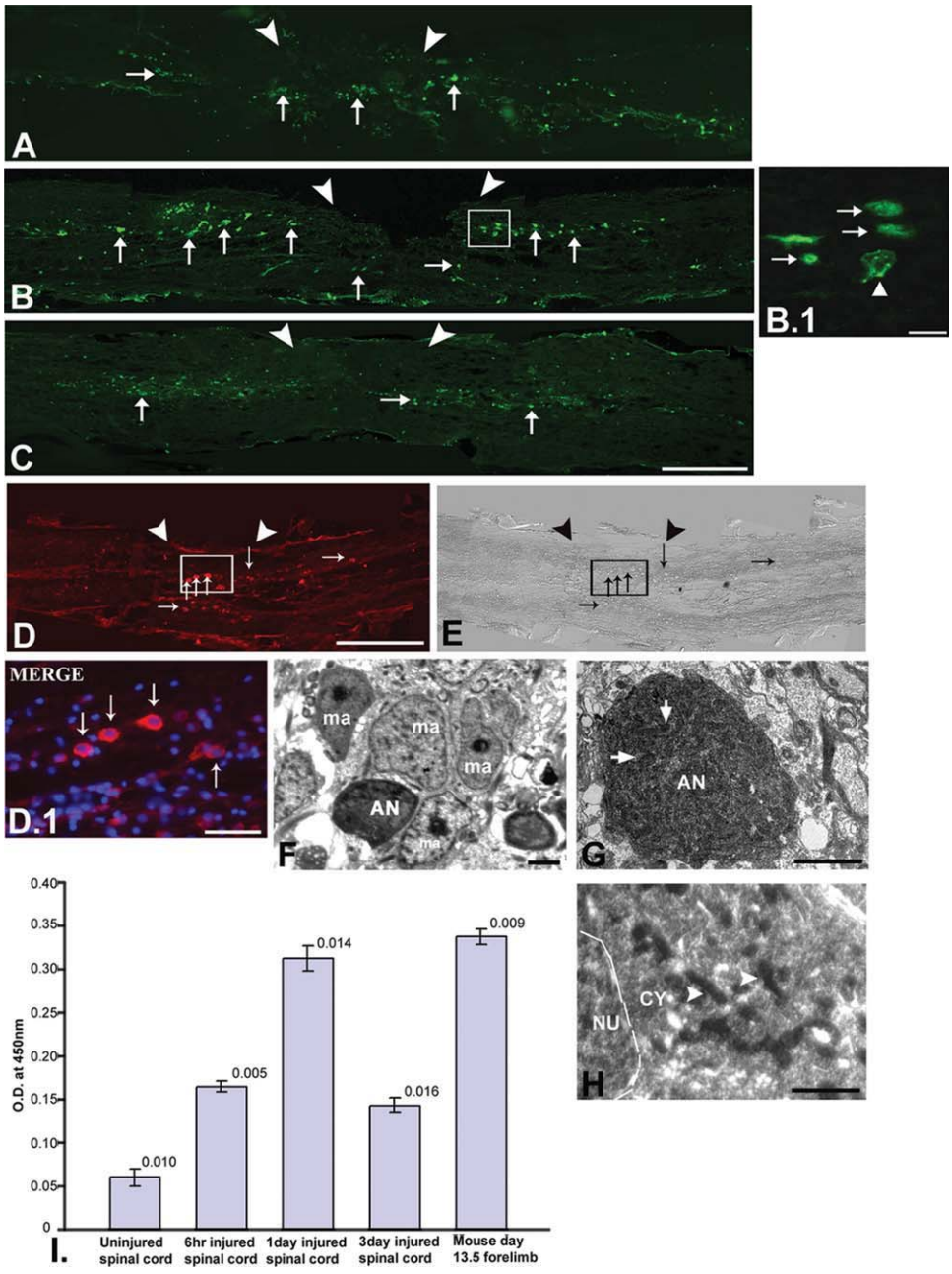

Fig. 8. TUNEL staining (A–C), caspase-3 immunohistochemistry (D–E), ultrastructural analysis (F–H), and quantification of caspase-3 (I) in injured zebrafish spinal cord. **A:** The 6-hr post-injured spinal cord section shows the presence of apoptotic TUNEL-positive cells (thin arrow) both at the injury epicenter (▼▼) and immediate adjacent part. **B:** The 1dpi cord shows many TUNEL-positive cells (thin arrow) close to the injury epicenter. **B.1:** The higher magnification picture of B shows many apoptotic cells (thin arrow) and a cell with fragmented nuclear matter (up white arrowhead). **C:** The 3dpi cord section shows less TUNEL-positive cells (thin arrow) compared to 1dpi cord. **D, E:** 1dpi cord section shows the presence of many caspase-3-positive apoptotic cells (thin arrow) at the injury epicenter with respective DIC. **D.1:** Higher magnification of same section shows some caspase-3 positive cells (thin arrow). **F–H:** Representative pictures of different apoptotic neurons in 3dpi cord, showing apoptotic neuron (AN) surrounded by macrophages (ma, F), another showing a fragmented nucleus (thick arrow) and retracted cytoplasm (G), and a third showing dying mitochondria (right white arrowhead) within the cytoplasm (H). **I:** Quantification of caspase-3 protein in uninjured and injured zebrafish spinal cord. Mouse day-13.5 forelimb represented positive control. Scale bar = 200 μm (A–E), 50 μm (D.1), 10 μm (B.1), 2 μm (F,G), 1 μm (H).

and mammalian cord and (2) what are the neuroprotective and regenerative responses following SCI in adult zebrafish. We observed hemorrhage, tissue edema, blood cell infiltration, and loss of neurons and glia following SCI. There is an influx of so-called inflammatory cells, like neutrophils, monocytes, and macrophages immediately after injury. As in mammals, these events occur early after injury but do not continue for long. Macrophages are important contributors of inflammatory response in mammals and may have both neuroprotective and neurodegenerative role in spinal cord injury and repair (Bethea, 2000; Shechter et al., 2009) because of the presence of distinctly different

populations of pro-inflammatory and anti-inflammatory macrophages (Kigerl et al., 2009, Shechter et al., 2009).

In the case of zebrafish, phagocytic macrophages accumulate at the lesion site 3 days after injury and continue to stay in decreasing numbers at 10dpi cord. These cells are involved in clearing cellular debris like dying neurons and damaged axons that may contain axonal inhibitory molecules as myelin breakdown products, probably causing suppression of an inflammatory response. Phagocytic macrophage activation enhances myelination by playing an important role in myelin debris removal, which is usually generated during demyelination. A previous report based on the spatio-temporal distribution of microglia/macrophage in injured fish brain suggested their possible role in clearance of apoptotic cells indirectly (Zupanc et al., 2003). Our ultrastructure analysis provided more definite evidence that the macrophages are indeed clearing myelin debris and apoptotic neurons. Thus it is possible that all the beneficial properties of macrophages, like secretion of neurotrophic factors (our unpublished observation), debris clearance through phagocytosis, and promotion of remyelination could contribute to an efficient repair process in zebrafish spinal cord after injury.

Ependymal Sealing Is a Regenerative Response, an Important Criterion of Successful Spinal Cord Regeneration

The initiation of regenerative response is observed as an accumulation of cells at the injury site and ependymal sealing in regenerating zebrafish spinal cord. Ependymal sealing can be seen in both crush and transection injury (data not shown) in zebrafish. A similar mechanism of migration and accumulation of cells here may also involve epithelial to mesenchymal transition as observed by O'Hara et al. (1992) and Chernoff (1996) in urodele. Sealing of ependyma during spinal cord regeneration was also confirmed in other regeneration-competent species in both adult and larval stages (Ferretti et al., 2003, Zhang et al., 2003, Chernoff et al., 2003). It is thought to be a common process both in tail amputation and spinal cord transection in urodeles (Butler and Ward, 1967; Singer et al., 1979; Stensaas, 1983). In the case of zebrafish, even crush injury, which involves ependymal disruption, can cause ependymal sealing and formation of the ependymal bulb. Our evidence also suggests the importance of ependymal sealing in spinal cord regeneration, since it was shown in an earlier study that delayed and imperfect sealing of ependyma at the lesion site by ependymal cells is an important contributing factor leading to loss of the regeneration capacity of post-metamorphic frog after telencephalic injury (Yoshino and Tochinai, 2004).

Demyelination and Remyelination, Role of the Schwann Cell

Following injury, axons are severed and cells in the white matter may die. Ultrastructural analysis and luxol fast blue staining confirm demyelination of axons following injury, causing severe loss of functions and thus we observed paralysis of the posterior part of the body and loss of swimming movements. We observed the extensive presence of Schwann cells at the injury site, which are dividing and indeed remyelinating denuded axons through basal membrane in regenerating cord. At least some of the regenerated axons showed remyelination by Schwann cells, which have contributed to functional recovery. A similar role of Schwann cells in myelination was also reported previously in injured goldfish optic nerve (Nona et al., 2000). Schwann cells of unknown origin are thought to infiltrate the lesion site, which gives rise to peripheral-type myelination in the regenerated optic nerve (Nona et al., 1994). We cannot confirm the origin or source of Schwann cells in regenerating zebrafish spinal cord but dividing Schwann cells are present around the demyelinated axons, which are known to be essential for the onset of myelination (Nona et al., 2000).

Apoptotic Cell Death

Secondary injury mechanism can lead to apoptotic cell death and contribute to both neuronal and glial loss in mammalian cord (Liu et al., 1997; Li et al., 1999; Newcomb et al., 1999). Time course analysis of two different apoptotic markers in zebrafish injured cord revealed induction of apoptotic cell death as early as 6 hr following injury with the highest level seen at 1dpi, and this is similar to what is observed in mammalian SCI (McEwen and Springer, 2005). Subsequently, there is a reduced level of cell death in injured fish cord, unlike mammals where caspase-3 expression continues until 8dpi (McEwen and Springer, 2005). Ultrastructural analysis showed the presence of an apoptotic body in the nucleus and dying mitochondria, which are considered to be typical characteristic features of apoptotic neurons, thus confirming neuronal apoptosis following injury. Although apoptotic cell death involves both grey matter and white matter, the extent of cell death is much greater in grey matter compared to white matter.

Previously, cell death in post-embryonic fish CNS was considered to be nonexistent (Fox and Richardson, 1982; Fine, 1989; Waxman and Anderson, 1985). Another report later showed that apoptotic cell death is required to control the cell proliferation in cerebellum (Soutschek and Zupanc, 1996). In adult teleost brain, apoptotic cell death occurs during neuronal regeneration (Zupanc et al., 1998), which leads to rapid removal and clearance of damaged cells, consequently augmenting the regeneration process. Until now, there has been no report of apoptotic cell death in zebrafish spinal cord. Our data confirm that injured spinal cord involves an apoptotic mechanism of debris clearance similar to that of brain and thus inhibits the progression of secondary degeneration after injury.

Injury-Induced Proliferation and Neurogenesis

We observed significant injury-induced proliferation in zebrafish spinal cord after being injured as reported by Reimer et al. (2008). However, temporal sequence of injury-induced proliferation in our study differs from their observation probably because of the variation in the nature of the injury induced since we have used crush injury as compared to transection. Cells around the ependyma and subependyma include both neuronal and radial glial cells and show a higher rate of BrdU

incorporation and H3P$^+$ cells, suggesting the contribution of both ependymal and subependymal cells in the regenerative process. Cells immediately around the ependymal canal (i.e., ventricular zone) represent the highest rate of proliferation as reported by us and others (Reimer et al., 2008). Proliferation may also involve white matter cells, but at a very low level. Uninjured cord reveals very few proliferating cells and injury causes significant proliferation as early as day 3 post-injury, which continues to rise until day 7 and declines at later time points. There is also a regional variation of proliferation; it involves both injury epicenter and the adjacent part of the cord as evidenced by both BrdU incorporation and H3P$^+$ cells. Initiation of proliferation starts at the site of injury as well as away from the stump and later proliferating cells migrate towards injury epicenter. Previous work in urodele spinal cord mentioned that the proliferation involves ependymal tissue somewhat distant to the plane of amputation (Egar and Singer, 1972; Nordlander and Singer 1978; Zhang et al., 2000) and that there was the presence of migrating proliferating precursors (Ferretti et al., 2003). We confirm injury-induced proliferative response as observed by others (Egar and Singer, 1972; Nordlander and Singer, 1978; Zhang et al., 2000; Monaghan et al., 2007) and proliferation as a key event in initiation and maintenance of regenerative response in zebrafish spinal cord.

Role of Radial Glia as Progenitor and in Dedifferentiation

Radial glial cells have distinct morphological features and well-defined glial characteristics (Holder et al., 1990; Cameron and Rakic, 1991) and are the most widespread non-neuronal cell type in developing CNS. There is a renewed attention to these cells, because of their ever increasing role in developmental processes including their function as neuronal precursors (Campbell and Gotz, 2002). These cells persist in adulthood in CNS of non-mammalian vertebrates ranging from fish to bird (Alvarez-Buyella et al., 2002; Kalman, 2002; Garcia-Verdugo et al., 2002; Zupanc and Clint, 2003) and most interestingly they remain in the areas where constitutive adult neurogenesis is an established phenomenon. Adult uninjured zebrafish cords have radial glia and astrocytes and do express GFAP. However, the radial glial population can be readily recognized (either dividing or nondividing) because of their obvious morphological characteristics, BrdU$^+$ nucleus during division, and soma of these cells that are located around the ependyma. Among the total population of radial glial cells, 1.2–1.6% is proliferating and present in both uninjured and injured cord. These particular populations of GFAP$^+$/BrdU$^+$ cells are probably neurogenic and are slowly dividing.

There is a decrease of GFAP expression immediately after injury and lack of expression of GFAP could not be attributed to loss of tissue due to injury since both 3dpi and 7dpi cord showed some accumulation of cells around the injury epicenter. Observation by others confirms a similar nature of expression of GFAP where they showed initial loss after injury followed by an increased level of expression at later time points in urodele cord (O'Hara et al., 1992; Chernoff et al., 2003).

We observed injury-induced proliferation and a higher percentage of proliferating precursors were GFAP$^-$/BrdU$^+$ in 3dpi and 7dpi cord. This population may refer to the importance of an early dedifferentiation process, which is followed by proliferation. These GFAP$^-$/BrdU$^+$ cells are fast dividing and represent the highest percentage of proliferating cells after injury. They could represent dedifferentiating cells and hence do not express differentiation markers of radial glia. A similar response of GFAP$^+$ astrocytes to mechanical injury was reported in mammalian brain (Hampton et al., 2004) where an initial dip in GFAP$^+$ cells does not represent the loss of astrocytes but confirms the presence of GFAP$^-$ astrocytes that are actually dedifferentiated and proliferating. Others interpreted the absence of GFAP after stab wounds in mammals as the presence of proliferating glial precursors (Alonso, 2005) that would differentiate into mature astrocytes.

The third population, which is GFAP$^+$/BrdU$^-$, consists of nonproliferating radial glia present in uninjured cord at a higher level than injured cord. A subset of this particular population may become GFAP$^-$/BrdU$^+$ after injury, when they are dedifferentiating and we see a drop in GFAP expression, followed by the reappearance of the same percentage of GFAP$^+$/BrdU$^-$ cells at 15dpi. There is the presence of both slow- and fast-dividing radial glia in zebrafish cord, of which a slow-dividing self-renewing population exists both in injured and uninjured cord, whereas a higher percentage of fast-dividing cells are represented in injured cord initially. Fast-dividing radial glia may divide symmetrically, generating cells of specific lineage. Thus, the importance of radial glia as precursors is enormous, since these cells can ideally generate both glial and neuronal populations and maintain the radial glial pool through self-renewal (Pinto and Gotz, 2007) as happens in cortical neurogenesis. Radial glial cells proliferate throughout vertebrate neurogenesis and identity of their progeny may vary (Hartfuss et al., 2001; Malatesta et al., 2000; Miyata et al., 2001). In urodeles, the radial glia generate diverse lineages and thus form glia, neurons, and neural crest cells after amputation of the adult tail (Echeverri and Tanaka, 2002).

Neurogenesis and Neuronal Differentiation

Fish CNS is capable of neurogenesis in adult life after injury and shows a remarkable ability for neural regeneration (Zupanc, 1999, 2001; Zupanc et al., 2005; Reimer et al., 2008). Studies on neurogenesis in spinal cord are still scarce (Kaslin et al., 2008) and little is known about the origin, fate, and differentiation of the produced cells, their survival as well as functional integration. Our data indicate substantial loss of neurons at the injury site immediately after injury and these cells are replaced during the process of regeneration in the same site as evidenced by histology, ultrastructural analysis, and expression of neuronal precursor markers. Expression of Hu protein in the cells present at the injury

epicenter marks the presence of newly committed early postmitotic neuronal cells, and also those cells that have just left the cell cycle (Hu^+/$Brdu^+$). These cells are present in greater number in the injury epicenter and are phenotypically different from Hu^+ cells in uninjured cord as confirmed by ultrastructural analysis and are contributing to neurogenesis in the regenerating cord. Initially, the same Hu^+ cells are not determined and hence $NeuroD^-$. Later on in 10dpi cord, at least some of these Hu^+ cells would become neuronally determined and $NeuroD^+$. We also observe that few Hu^+/$NeuroD^+$ cells are present in the ventricular zone of the ependyma in both the injury epicenter and in the immediate adjacent parts, and would probably migrate to acquire a subependymal position and integrate into a fully regenerated cord. Some cells are also appropriately present in the subependyma showing projections and integrated into the regenerating cord. Subpial location of newly generated neurons can also be seen in the injured cord. Similar reports on post-embryonic zebrafish brain (Mueller and Wullimann, 2002) showed subpial neurogenesis, where there is high neuronal plasticity suggesting injury-induced neurogenesis in zebrafish cord.

The radial glia undergoes asymmetric division to generate neurons during cortical neurogenesis (Pinto and Gotz, 2007), whereas radial glia in transected adult fish cord generates motor neurons (Reimer et al., 2008). We observed neurogenesis in injured spinal cord and a subset of radial glial population are, indeed, slowly dividing, which may generate new neurons through asymmetric division. Since the newly formed neurons are coming from both fast- and slow-dividing cells, it is possible that these cells are coming from asymmetrically dividing radial glia and a higher percentage of fast-dividing population may have generated from symmetric division, and include different neuronal progenitors.

Our data suggest that in adult regenerating spinal cord, both proliferating neuronal precursors (Hu^+/$Brdu^+$) and neuronally determined cells (Hu^+/$NeuroD^+$) are present in the injury epicenter and immediate adjacent parts of the injury epicenter suggestive of neurogenesis in both these regions. The presence of newly formed neurons (Hu^+/$BrdU^+$) after injury is more evident because of their morphology. They are small round cells with a large nucleus and relatively small cytoplasm containing new but fewer organelles, a typical characteristic of newly formed neurons, as confirmed by ultrastructural analysis (Alvarez-Buylla et al., 1998).

In conclusion, we are the first to characterize the injury-induced cellular responses in zebrafish spinal cord. Unlike mammals, some of these responses do not contribute to secondary degeneration like apoptotic cell death and macrophage invasion and others contribute to the creation of a permissive environment for regeneration. Proliferative response after injury is crucial and our study shows that SCI can lead to generation of new neurons as well as their time course and differentiation during regeneration. We showed the role of radial glia as proliferating precursor in neurogenesis. In the future, it will be important to study the role of signaling molecules for the creation of a regeneration permissive environment. Intense characterization of precursor cells needs to be done in order to elucidate the molecular basis of regeneration.

EXPERIMENTAL PROCEDURES

Fish Maintenance

Zebrafish of approximately of 3–4 cm in length were obtained either from a local pet shop or bred in our animal house facility. Fish were kept in separate groups of 10 in the aquatic system maintained at 28°C on a 14-hr light/10-hr dark cycle.

Surgical Procedures for Inflicting Spinal Cord Injury to Adult Fish

Fishes were anaesthetized for 5 min in 0.02% tricaine (MS222; Sigma, St. Louis, MO) before giving spinal cord injury (SCI). A longitudinal lesion was made at the side of the fish to expose the vertebral column at the level of the dorsal fin, which corresponds to the 15–16th vertebrae as confirmed by skeletal preparation. The spinal cord was crushed by dorso-ventral crushing for 1 sec with a number-5 Dumont forceps. Giving a suture later sealed wounds and fishes were allowed to regenerate at 28°C for different time periods.

BrdU Incorporation

We injected 50 μl volume of BrdU (Bromo-deoxy- Uridine, Sigma-Aldrich) at the concentration 2.5 mg/ml to adult fish intraperitoneally, 16 hr before the collection of tissues at different time points. To detect the slow cycling cells, we have used continuous BrdU pulse for the first 48 hr after injury and then chased the same fish until day 7. A spinal cord tissue equivalent to approximately 4 mm length was collected from both injured and uninjured animals. Tissue samples from injured cord were collected in such a way that the epicenter of the lesion was placed at the middle of the cord and included normal tissues on both sides of the injury. Tissues were processed for BrdU immunohistochemistry and labeled cells were counted in the sections of approximately 4 mm length from both injured and uninjured spinal cord.

Histology, Transmission Electron Microscopy (TEM), and Immunohistochemistry

Spinal cord tissues were dissected out and fixed in 4% paraformaldehyde (Sigma) for 8 hr or overnight at 4°C. Both injured and uninjured spinal cord tissues were embedded either in paraffin or in a mixture of PEG and hexadecanol (9:1, Sigma) or in O.C.T compound (Leica) and sectioned at 5–7 μm. For routine histology, sections were stained either with hematoxylin and eosin (H&E), Mallory's trichrome stain (Humason, 1979), or luxol fast blue and cresyl violet.

For TEM, both normal and injured adult spinal cords were dissected out from bony skeleton and 2-mm-length tissue was excised from whole spinal cord containing injury epicenter in case of injured tissue. Tissues were quickly fixed in Karnovsky's fixative for 12 hr in 4°C (David et al., 1973). After washing with 0.2M phosphate buffer (pH 7.4), tissues were osmicated in 1% OsO_4 in 0.01M phosphate buffer

and embedded in Araldite CY212. Ultrathin sections (70 nm) were cut using an ultramicrotome (Leica, Wetzlar, Germany) and were stained with uranyl acetate and lead citrate and viewed under a Morgagni 268D electron microscope (Fei Company, Eindhoven, Netherlands) using a multihole grid.

Immunostaining was performed as described previously (Ferretti and Ghosh, 1997) by using the following primary antibodies shown to specifically recognize fish, amphibian, and human protein: anti glial fibrillary acidic protein (GFAP), rabbit polyclonal antibody (1:500, DAKO, Carpinteria, CA), anti-β III Tubulin, mouse monoclonal antibody (1:50, Sigma), anti-BrdU (1:400, Sigma), anti caspase-3 goat polyclonal (1:100, Santa Cruz Biotechnology, Santa Cruz, CA), anti NeuroD (1:100, Santa Cruz), and anti Hu C/D (1:50, Molecular Probes, Eugene, OR). Briefly, sections were rehydrated and given several washes in Phosphate buffered saline (PBS) with 0.1% Tween-20 or Triton X 100 (PBST). The sections were first incubated with blocking solution for 1 hr (5% goat/rabbit/donkey serum, 1% BSA in PBS) and then with primary antibody for either 1 hr at room temperature or overnight at 4°C. Antigen retrieval was done wherever appropriate by keeping the slides in 80°C water bath for 15 min either in sodium-citrate buffer (pH 6.0) or Tris buffer (pH 8.0) before incubation with the primary antibody.

The following secondary antibodies were used: Rhodamine-conjugated goat anti-rabbit antibody (1:100, Santa Cruz), rhodamine-conjugated donkey anti-goat antibody (1:100, Santa Cruz), rhodamine-conjugated goat anti-rabbit IgG antibody (1:100, Jackson ImmunoResearch Laboratories, West Grove, PA), and FITC-conjugated goat anti-mouse (1:50, Santa Cruz). Nuclei were counter-stained either with bisbenzimide H 33258 fluorochrome (Hoechst nuclear stain) or with DAPI (1: 500, Sigma).

BrdU immunohistochemistry on uninjured and injured spinal cord was done according to Mueller and Wullimann (2002). Paraformaldehyde-fixed paraffin sections were washed in PBST twice for 10 min, followed by incubation in 2N HCl (pH 2.0) for 30 min at 37°C. Sections were washed in PBS and blocked with 5% normal goat serum in 0.5% PBST for 1 hr at room temperature. The mouse monoclonal anti-BrdU primary antibody (1:400, Sigma) was applied for 2 hr at room temperature or overnight at 4°C. This was followed by washes in PBS and incubated with secondary anti-mouse FITC/TRITC conjugated antibody for 2 hr at room temperature. After washing in PBS, the sections were mounted with Aqua Vectashield (Vector Labs, Burlingame, CA) and kept in the dark.

TdT-Mediated Deoxy-UTP-Nick End Labeling (TUNEL) Assay

TUNEL staining was performed to detect apoptotic cells using the "In Situ Cell Death Detection Kit, Fluorescein" (Roche Molecular Biochemicals, Mannheim, Germany). In brief, deparaffinized sections were permeabilized in PBS containing 0.02% Triton X-100 for 10 min. After washing in PBS for 10 min, tissue sections were incubated with TUNEL reaction mixture for 2 hr at 37°C. After several washings in PBS, sections were mounted by vectashield and examined under confocal microscope. The morphological changes of nuclei were also examined to clear the visualization of apoptotic bodies.

Microscopy

The light microscopic photographs were taken by using a Leica DMLB microscope. Immunostained tissue sections were photographed by using an Olympus fluorescent microscope (model; BX 51) with Imagepro express software and confocal images were obtained by using a Zeiss LSM 510 Meta (inverted) confocal microscope. Figures were assembled and edited with Adobe Photoshop CS and Image Ready software packages.

ELISA

Analysis of Caspase-3 protein by using ELISA assay was done according to Dutta et al. (2009). Tissue extract of spinal cord were added to wells (65 μg protein/well) of the ELISA plate and incubated overnight at 4°C. After nonspecific sites were blocked with blocking buffer (1% BSA in PBS), the wells were incubated with primary antibody (anti-Caspase-3) for 1 hr at 37°C, and washed thrice in washing buffer (0.5% BSA, 0.5% NP-40 in PBS). HRP coupled anti-goat antibody (1:1,000 dilution) was used for incubating the plates at 37°C for 1 hr, then washed several times in washing buffer and substrate TMB (tetramethyl benzedine) was added in dark. The reaction was stopped by adding 1M H_2SO_4. The optical density was measured at 450 nm by using an ELISA reader (Bio Rad, Gaithersburg, MD).

Measurement of Functional Locomotor Activity

Motor function activity has been studied both in uninjured and injured fishes by monitoring the swimming behavior and pattern of individual fish. Both the distance covered and directional changes were recorded by placing the fish in a container with a uniform grid length (about 9 cm) and a constant water level, temperature, and light source were maintained during all the experiments. Fishes of same size (approximately 3 cm) and age were used for all experiments. The functional behavior of the fishes at different time points (3dpi, 7dpi, 10dpi, 15dpi, and 1 month post-injury) were recorded several times a day for 3 min in each run. Initially, before giving spinal cord injury, the swimming activity and traveled distance for all the uninjured fishes were measured. The bar graph was constructed using the mean value of swimming distance covered in each time point and the variability of values is given as SEM.

Quantification and Statistical Analysis

For BrdU incorporation experiment, $BrdU^+$ cells were counted in longitudinal spinal cord section by using an Olympus fluorescent microscope (model; BX 51). During quantification, $BrdU^+$ cells in both grey and white matter region were counted; slow- and fast-dividing cells were differentiated according to their staining intensities. In GFAP and BrdU colocalization study, the quantification of cells was done from all optical images by using a Zeiss LSM 510 Meta (inverted)

confocal microscope. We have used approximately 4-mm length of tissues both from uninjured and injured cords, sectioned the whole cord, and all the sections were stained with GFAP (to count $GFAP^+$ cells representing radial glial morphology, the soma of the radial glia was positioned towards ependymal canal) and DAPI (to count nucleus) along with BrdU staining. The statistical analyses were performed with Microsoft Excel (Office 2000) and variability of values is given as SEM. Statistical significance was determined using an unpaired Student's *t*-test and Mann-Whitney U-test. Results were considered statistically significant at $P < 0.05$ for both tests.

ACKNOWLEDGMENTS

We thank Dr. T. K. Nag, AIIMS, for his excellent technical assistance and guidance to generate Electron microscopy data. This work was supported by the Department of Biotechnology, Ministry of Science and Technology, Govt. of India, to Sukla Ghosh. S. P. Hui is a recipient of a senior research fellowship from the Council of Scientific and Industrial Research, Govt. of India.

REFERENCES

Alonso G. 2005. NG2 proteoglycan-expressing cells of the adult rat brain: possible involvement in the formation of glial scar astrocytes following stab wound. Glia 49:318–338.

Alvarez-Buylla A, Garcia-Verdugo JM, Mateo AS, Merchant-Larios H. 1998. Primary neural precursors and intermitotic nuclear migration in the ventricular zone of adult canaries. J Neurosci 18:1020–1037.

Alvarez-Buylla A, Seri B, Doetsch F. 2002. Identification of neural stem cells in the adult vertebrate brain. Brain Res Bull 57:751–758.

Anderson MJ, Waxman SG. 1983. Caudal spinal cord of the teleost *Sternarchus albifrons* resembles regenerating cord. Anat Rec 205:85–92.

Appel B, Chitnis A. 2002. Neurogenesis and Specification of Neuronal Identity. In: Solnica-Krezel L, editor. Pattern formation in zebrafish, Heidelberg: Springer-Verlag. p 237–251.

Balentine JD. 1978a. Pathology of experimental spinal cord trauma. I. The necrotic lesion as a function of vascular injury. Lab Invest 39:236–253.

Balentine JD. 1978b. Pathology of experimental spinal cord trauma. II. Ultrastructure of axons and myelin. Lab Invest 39:254–266.

Beattie MS, Farooqui AA, Bresnahan JC. 2000. Review of current evidence for apoptosis after spinal cord injury. J Neurotrauma 17:915–925.

Becker T, Wullimann MF, Becker CG, Bernhardt RR, Schachner M. 1997. Axonal regrowth after spinal cord transection in adult zebrafish. J Comp Neurol 377:577–595.

Becker T, Lieberoth BC, Becker CG, Schachner M. 2005. Differences in the regenerative response of neuronal cell populations and indications for plasticity in intraspinal neurons after spinal cord transection in adult zebrafish. Mol Cell Neurosci 30:265–278.

Bernhardt RR. 1999. Cellular and molecular bases of axonal regeneration in the fish central nervous system. Exp Neurol 157:223–240.

Bethea JR. 2000. Spinal cord injury-induced inflammation: a dual-edged sword. Prog Brain Res 128:33–42.

Blight AR. 1985. Delayed demyelination and macrophage invasion: a candidate for secondary cell damage in spinal cord injury. Cent Nerv Syst Trauma 2:299–315.

Butler EG, Ward MB. 1967. Reconstitution of the spinal cord after ablation in adult Triturus. Dev Biol 15:464–486.

Cameron RS, Rakic P. 1991. Glial cell lineage in the cerebral cortex: a review and synthesis. Glia 4:124–137.

Campbell K, Gotz M. 2002. Radial glia: multi-purpose cells for vertebrate brain development. Trends Neurosci 25: 235–238.

Chernoff EA. 1996. Spinal cord regeneration: a phenomenon unique to urodeles? Int J Dev Biol 40:823–831.

Chernoff EA, Stocum DL, Nye HL, Cameron JA. 2003. Urodele spinal cord regeneration and related processes. Dev Dyn 226:295–307.

Citron BA, Arnold PM, Sebastian C, Qin F, Malladi S, Ameenuddin S, Landis ME, Festoff BW. 2000. Rapid upregulation of caspase-3 in rat spinal cord after injury: mRNA, protein, and cellular localization correlates with apoptotic cell death. Exp Neurol 166:213–226.

Crowe MJ, Shuman SL, Masters JN, Bresnahan JC, Beattie MS. 1995. Morphological evidence suggesting apoptotic nuclei in spinal cord injury. Soc Neurosci Abstr 21:232.

David E, Winkelmann E, Marx I, David H. 1973. Ultrastructural changes of neurons and synapses in the neocortex, striatum, and thalamus induced by oxygen deficiency in the guinea pig (*Cavia porcellus* L.). J Hirnforsch 14:375–388.

Donnelly DJ, Popovich PG. 2008. Inflammation and its role in neuroprotection, axonal regeneration and functional recovery after spinal cord injury. Exp Neurol 209:378–388.

Dutta A, Sen T, Banerji A, Das S, Chatterjee A. 2009. Studies on multifunctional effect of all-trans retinoic acid (ATRA) on matrix metalloproteinase-2 (MMP-2) and its regulatory molecules in human breast cancer cells (MCF-7). J Oncol 2009:627840.

Echeverri K, Tanaka EM. 2002. Ectoderm to mesoderm lineage switching during axolotl tail regeneration. Science 298: 1993–1996.

Egar M, Singer M. 1972. The role of ependyma in spinal cord regeneration in the urodele, Triturus. Exp Neurol 37:422–430.

Ferretti P, Ghosh S. 1997. Expression of regeneration-associated cytoskeletal proteins reveals differences and similarities between regenerating organs. Dev Dyn 210:288–304.

Ferretti P, Zhang F, O'Neill P. 2003. Changes in spinal cord regenerative ability through phylogenesis and development: lessons to be learnt. Dev Dyn 226:245–256.

Fine ML. 1989. Embryonic, larval and adult development of the sonic neuromuscular system in the oyster toadfish. Brain Behav Evol 34:13–24.

Fitch MT, Doller C, Combs CK, Landreth GE, Silver J. 1999. Cellular and molecular mechanisms of glial scarring and progressive cavitation: in vivo and in vitro analysis of inflammation-induced secondary injury after CNS trauma. J Neurosci 19:8182–8198.

Fox GQ, Richardson GP. 1982. The developmental morphology of *Torpedo marmorata*: electric lobe-electromotoneuron proliferation and cell death. J Comp Neurol 207:183–190.

Gage FH. 2000. Mammalian neural stem cells. Science 287:1433–1438.

Garcia-Verdugo JM, Ferron S, Flames N, Collado L, Desfilis E, Font E. 2002. The proliferative ventricular zone in adult vertebrates: a comparative study using reptiles, birds, and mammals. Brain Res Bull 57:765–775.

Guth L, Zhang Z, Steward O. 1999. The unique histopathological responses of the injured spinal cord. Implications for neuroprotective therapy. Ann NY Acad Sci 890:366–384.

Hampton DW, Rhodes KE, Zhao C, Franklin RJ, Fawcett JW. 2004. The responses of oligodendrocyte precursor cells, astrocytes and microglia to a cortical stab injury, in the brain. Neuroscience 127:813–820.

Hartfuss E, Galli R, Heins N, Gotz M. 2001. Characterization of CNS precursor subtypes and radial glia. Dev Biol 229:15–30.

Holder N, Clarke JD, Kamalati T, Lane EB. 1990. Heterogeneity in spinal radial glia demonstrated by intermediate filament expression and HRP labelling. J Neurocytol 19:915–928.

Humason GL. 1979. Animal tissue techniques. New York: WH Freeman & Co.

Kalman M. 2002. GFAP expression withdraws: a trend of glial evolution? Brain Res Bull 57:509–511.

Kaslin J, Ganz J, Brand M. 2008. Proliferation, neurogenesis and regeneration in the non-mammalian vertebrate brain. Phil Trans R Soc Lond B Biol Sci 363:101–122.

Kigerl KA, Gensel JC, Ankeny DP, Alexander JK, Donnelly DJ, Popovich PG. 2009. Identification of two distinct

macrophage subsets with divergent effects causing either neurotoxicity or regeneration in the injured mouse spinal cord. J Neurosci 29:13435–13444.
Kim CH, Ueshima E, Muraoka O, Tanaka H, Yeo SY, Huh TL, Miki N. 1996. Zebrafish elav/HuC homologue as a very early neuronal marker. Neurosci Lett 216:109–112.
Korzh V, Sleptsova I, Liao J, He J, Gong Z. 1998. Expression of zebrafish bHLH genes ngn1 and nrd defines distinct stages of neural differentiation. Dev Dyn 213:92–104.
Leonard RB, Coggeshall RE, Willis WD. 1978. A documentation of an age related increase in neuronal and axonal numbers in the stingray, *Dasyatis sabina*, Leseuer. J Comp Neurol 179:13–21.
Li GL, Farooque M, Holtz A, Olsson Y. 1999. Apoptosis of oligodendrocytes occurs for long distances away from the primary injury after compression trauma to rat spinal cord. Acta Neuropathol 98:473–480.
Liu XZ, Xu XM, Hu R, Du C, Zhang SX, McDonald JW, Dong HX, Wu YJ, Fan GS, Jacquin MF, Hsu CY, Choi DW. 1997. Neuronal and glial apoptosis after traumatic spinal cord injury. J Neurosci 17:5395–5406.
Malatesta P, Hartfuss E, Gotz M. 2000. Isolation of radial glial cells by fluorescent-activated cell sorting reveals a neuronal lineage. Development 127: 5253–5263.
McEwen ML, Springer JE. 2005. A mapping study of caspase-3 activation following acute spinal cord contusion in rats. J Histochem Cytochem 53:809–819.
Miyata T, Kawaguchi A, Okano H, Ogawa M. 2001. Asymmetric inheritance of radial glial fibers by cortical neurons. Neuron 31:727–741.
Monaghan JR, Walker JA, Page RB, Putta S, Beachy CK, Voss SR. 2007. Early gene expression during natural spinal cord regeneration in the salamander *Ambystoma mexicanum*. J Neurochem 101:27–40.
Morshead CM, Reynolds BA, Craig CG, McBurney MW, Staines WA, Morassutti D, Weiss S, van der Kooy D. 1994. Neural stem cells in the adult mammalian forebrain: a relatively quiescent subpopulation of subependymal cells. Neuron 13:1071–1082.
Mueller T, Wullimann MF. 2002. BrdU-, neuroD (nrd)- and Hu-studies reveal unusual non-ventricular neurogenesis in the postembryonic zebrafish forebrain. Mech Dev 117:123–135.
Naganska E, Matyja E. 2001. Ultrastructural characteristics of necrotic and apoptotic mode of neuronal cell death in a model of anoxia in vitro. Folia Neuropathol 39:129–139.
Newcomb JK, Zhao X, Pike BR, Hayes RL. 1999. Temporal profile of apoptotic-like changes in neurons and astrocytes following controlled cortical impact injury in the rat. Exp Neurol 158:76–88.
Nona SN, Stafford CA, Duncan A, Cronly-Dillon JR, Scholes J. 1994. Myelin repair by Schwann cells in the regenerating goldfish visual pathway: regional patterns revealed by X-irradiation. J Neurocytol 23:400–409.
Nona SN, Thomlinson AM, Bartlett CA, Scholes J. 2000. Schwann cells in the regenerating fish optic nerve: evidence that CNS axons, not the glia, determine when myelin formation begins. J Neurocytol 29:285–300.
Nordlander RH, Singer M. 1978. The role of ependyma in regeneration of the spinal cord in the urodele amphibian tail. J Comp Neurol 180:349–374.
O'Hara CM, Egar MW, Chernoff EA. 1992. Reorganization of the ependyma during axolotl spinal cord regeneration: changes in intermediate filament and fibronectin expression. Dev Dyn 193: 103–115.
Park HC, Hong SK, Kim HS, Kim SH, Yoon EJ, Kim CH, Miki N, Huh TL. 2000. Structural comparison of zebrafish Elav/Hu and their differential expressions during neurogenesis. Neurosci Lett 279:81–84.
Pinto L, Gotz M. 2007. Radial glial cell heterogeneity: the source of diverse progeny in the CNS. Prog Neurobiol 83: 2–23.
Popovich PG, Wei P, Stokes BT. 1997. Cellular inflammatory response after spinal cord injury in Sprague-Dawley and Lewis rats. J Comp Neurol 377:443–464.
Reimer MM, Sorensen I, Kuscha V, Frank RE, Liu C, Becker CG, Becker T. 2008. Motor neuron regeneration in adult zebrafish. J Neurosci 28:8510–8516.
Reimer MM, Kuscha V, Wyatt C, Sorensen I, Frank RE, Knuwer M, Becker T, Becker CG. 2009. Sonic hedgehog is a polarized signal for motor neuron regeneration in adult zebrafish. J Neurosci 29:15073–15082.
Renault-Mihara F, Okada S, Shibata S, Nakamura M, Toyama Y, Okano H. 2008. Spinal cord injury: emerging beneficial role of reactive astrocytes' migration. Int J Biochem Cell Biol 40: 1649–1653.
Shechter R, London A, Varol C, Raposo C, Cusimano M, Yovel G, Rolls A, Mack M, Pluchino S, Martino G, Jung S, Schwartz M. 2009. Infiltrating blood-derived macrophages are vital cells playing an anti-inflammatory role in recovery from spinal cord injury in mice. PLOS Med 6:1–17.
Shuman SL, Bresnahan JC, Beattie MS. 1996. Morphological evidence of glial involvement in apoptotic cell death following spinal cord contusion. Soc Neurosci Abstr 22:1185.
Singer M, Nordlander RH, Egar M. 1979. Axonal guidance during embryogenesis and regeneration in the spinal cord of the newt: the blueprint hypothesis of neuronal pathway patterning. J Comp Neurol 185:1–21.
Song HJ, Stevens CF, Gage FH. 2002. Neural stem cells from adult hippocampus develop essential properties of functional CNS neurons. Nat Neurosci 5: 438–445.
Soutschek J, Zupanc GK. 1996. Apoptosis in the cerebellum of adult teleost fish, *Apteronotus leptorhynchus*. Brain Res Dev Brain Res 97:279–286.
Stensaas LJ. 1983. Regeneration in the spinal cord of the newt *Notophthalmus* (Triturus) *pyrrhogaster*. In: Kao CC, Bunge RP, Reier PJ, editors. Spinal cord reconstruction. New York: Raven Press. p121–149.
Takagi T, Takayasu M, Mizuno M, Yoshimoto M, Yoshida J. 2003. Caspase activation in neuronal and glial apoptosis following spinal cord injury in mice. Neurol Med Chir 43:20–9.
Waxman SG, Anderson MJ. 1985. Generation of electromotor neurons in *Sternarchus albifrons*: differences between normally growing and regenerating spinal cord. Dev Biol 112:338–344.
Wilson SW, Brand M, Eisen JS. 2002. Patterning the zebrafish central nervous system. Results Prob Cell Differ 40: 181–215.
Yoshino J, Tochinai S. 2004. Successful reconstitution of the non regenerating adult telencephalon by cell transplantation in *Xenopus leavis*. Dev Growth Differentiation 46:523–534.
Zhang F, Clarke JD, Ferretti P. 2000. FGF-2 Up-regulation and proliferation of neural progenitors in the regenerating amphibian spinal cord in vivo. Dev Biol 225:381–391.
Zhang F, Ferretti P, Clarke JD. 2003. Recruitment of postmitotic neurons into the regenerating spinal cord of urodeles. Dev Dyn 226:341–348.
Zupanc GK. 1999. Neurogenesis, cell death and regeneration in the adult gymnotiform brain. J Exp Biol 202: 1435–1446.
Zupanc GK. 2001. Adult neurogenesis and neuronal regeneration in the central nervous system of teleost fish. Brain Behav Evol 58:250–275.
Zupanc GK, Clint SC. 2003. Potential role of radial glia in adult neurogenesis of teleost fish. Glia 43:77–86.
Zupanc GK, Horschke I. 1995. Proliferation zones in the brain of adult gymnotiform fish: a quantitative mapping study. J Comp Neurol 353:213–233.
Zupanc GK, Zupanc MM. 2006. New neurons for the injured brain: mechanisms of neuronal regeneration in adult teleost fish. Regen Med 1:207–216.
Zupanc GK, Kompass KS, Horschke I, Ott R, Schwarz H. 1998. Apoptosis after injuries in the cerebellum of adult teleost fish. Exp Neurol 152:221–230.
Zupanc GK, Clint SC, Takimoto N, Hughes AT, Wellbrock UM, Meissner D. 2003. Spatio-temporal distribution of microglia/macrophages during regeneration in the cerebellum of adult teleost fish, Apteronotus leptorhynchus: a quantitative analysis. Brain Behav Evol 62:31–42.
Zupanc GK, Hinsch K, Gage FH. 2005. Proliferation, migration, neuronal differentiation, and long-term survival of new cells in the adult zebrafish brain. J Comp Neurol 488:290–319.